

# Chiral charge order in $1T$ -TiSe<sub>2</sub>: importance of lattice degrees of freedom

B. Zenker<sup>1</sup>, H. Fehske<sup>1</sup>, H. Beck<sup>2</sup>, C. Monney<sup>3</sup>, and A. R. Bishop<sup>4</sup>

<sup>1</sup>*Institut für Physik, Ernst-Moritz-Arndt-Universität Greifswald, D-17489 Greifswald, Germany*

<sup>2</sup>*Département de Physique and Fribourg Center for Nanomaterials, Université de Fribourg, CH-1700 Fribourg, Switzerland*

<sup>3</sup>*Fritz-Haber-Institut der Max Planck Gesellschaft, Faradayweg 4-6, 14195 Berlin, Germany*

<sup>4</sup>*Theory, Simulation, and Computation Directorate, Los Alamos National Laboratory, Los Alamos, New Mexico 87545, USA*

(Dated: November 29, 2021)

We address the question of the origin of the recently discovered chiral property of the charge-density-wave phase in  $1T$ -TiSe<sub>2</sub> which so far lacks a microscopic understanding. We argue that the lattice degrees of freedom seems to be crucial for this novel phenomenon. We motivate a theoretical model that takes into account one valence and three conduction bands, a strongly screened Coulomb interaction between the electrons, as well as the coupling of the electrons to a transverse optical phonon mode. The Falicov-Kimball model extended in this way possesses a charge-density-wave state at low temperatures, which is accompanied by a periodic lattice distortion. The charge ordering is driven by a lattice deformation and electron-hole pairing (excitonic) instability in combination. We show that both electron-phonon interaction and phonon-phonon interaction must be taken into account at least up to quartic order in the lattice displacement to achieve a stable chiral charge order. The chiral property is exhibited in the ionic displacements. Furthermore, we provide the ground-state phase diagram of the model and give an estimate of the electron-electron and electron-phonon interaction constants for  $1T$ -TiSe<sub>2</sub>.

PACS numbers: 71.45.Lr, 71.27.+a, 63.20.kk, 71.35.Lk, 71.38.-k

## I. MOTIVATION

Charge-density-waves (CDWs) brought about by electron-phonon<sup>1</sup> or electron-electron<sup>2</sup> interactions are broken-symmetry ground states, typically of low-dimensional (D) solids with anisotropic properties.<sup>3</sup> A prominent material exhibiting such a periodic real-space modulation of its charge density is the transition-metal dichalcogenide  $1T$ -TiSe<sub>2</sub>. This quasi-2D system undergoes a structural phase transition at about 200 K, at which a commensurate  $2 \times 2 \times 2$  superstructure accompanied by a CDW develops.<sup>4</sup> Thereby the CDW features three coexisting components and, for this reason, is denoted as triple CDW. Although the charge-ordered phase in  $1T$ -TiSe<sub>2</sub> has been a matter of intensive research for more than three decades, the driving force behind the phase transition has not been identified conclusively.

Recent experiments on  $1T$ -TiSe<sub>2</sub>, pointing to a very unusual chiral property of the CDW, have reinforced the interest in this problem.<sup>5,6</sup> An object exhibits chirality if it cannot be mapped on its mirror image solely by rotations and translations. For a CDW phase characterized by a scalar quantity such as chirality has not been detected before. The scanning tunneling microscopy measurements performed by Ishioka and co-workers, however, show that the amplitude of the tunneling current modulates differently along the CDW unit vectors in  $1T$ -TiSe<sub>2</sub>.<sup>5</sup> Since the tunneling-current amplitude directly measures the local electron density, the charge density modulates differently along the three unit vectors. As a result the material in its low-temperature phase will not exhibit a three-fold symmetry as suggested by the triangular lattice structure. The Fourier transformation

of the scanning tunneling microscopy data demonstrates a triple CDW as well as a different charge modulation along each CDW component with the respective ordering vector  $Q_\alpha$ ,  $\alpha = 1, 2, 3$ .<sup>5</sup> If one orders the triple-CDW components according to their charge modulation amplitude in ascending order, in a sense a direction is singled out and the triple CDW exhibits chirality because the mirror symmetry is broken, in contrast to usual CDWs;<sup>6</sup> see the schematic representation by Fig. 1. Note that clockwise and anticlockwise chiral CDWs were found in the same sample, suggesting that these states are degenerate.

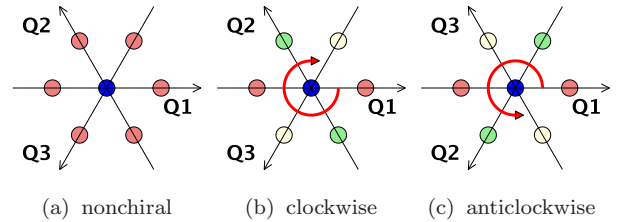


FIG. 1. (color online) Electron-density pattern for a triangular lattice in case of (a) a nonchiral CDW or (b,c) chiral CDWs. Filled circles picture the value of the charge densities, where equal colors mark equal densities. For the nonchiral CDW shown in (a) the density modulation along the ordering vectors  $Q_1$ ,  $Q_2$ , and  $Q_3$  is equal. Reflection along an ordering vector yields the same density pattern, i.e., mirror symmetry exists. The situation changes for a chiral CDW. A clockwise CDW (red arrow) is illustrated in (b). Now reflection along  $Q_1$  yields the situation depicted in panel (c). Obviously the pattern (c) describes an anticlockwise CDW: That is, for a chiral CDW mirror symmetry is broken.

erate. This two-fold symmetry is corroborated by optical polarimetry measurements.<sup>5</sup> Ishioka and co-workers furthermore noticed that the experimental data can be reproduced by a charge density modulation of the form

$$n_i(\mathbf{Q}_\alpha) = A \cos(\mathbf{Q}_\alpha \mathbf{R}_i + \theta_\alpha), \quad (1)$$

where  $A$  is the modulation amplitude and  $\theta_\alpha$  are initial phases.<sup>5</sup> For a chiral CDW to exist the phases of the CDW components must differ, i.e.,  $\theta_1 \neq \theta_2 \neq \theta_3$ .

From a theoretical point of view the chiral CDW in  $1T$ - $\text{TiSe}_2$  was addressed by a Landau-Ginzburg approach.<sup>7,8</sup> Thereby the relative phases of the CDW order parameters were obtained by minimizing the free energy functional. Two CDW transitions were found with decreasing temperature: Firstly a standard (nonchiral) CDW appears, and subsequently a chiral CDW emerges, i.e.,  $T_{\text{nonchiral CDW}} > T_{\text{chiral CDW}}$ . Within the CDW phase three distinct orbital sectors are occupied, leading to an orbital-ordered state and three interacting lattice displacement waves (with different polarizations).

An open issue is the microscopic mechanism driving the CDW transition. Basically two scenarios have been discussed in the literature, where the charge order results from purely electronic, respectively electron-lattice, correlations. Angle-resolved photoemission spectroscopy data reveal a relatively large transfer of spectral weight from the original bands to the back-folded bands (due to the CDW transition), compared with the small ionic displacement. This suggests an electronic mechanism within the excitonic insulator (EI) scenario.<sup>9,10</sup> A corresponding tight-binding calculation estimates the amplitude of the lattice deformation caused by an EI instability to be of the same order as the measured one.<sup>11</sup> The gradual suppression of the CDW phase by changing solely electronic properties by intercalation with S or Te further corroborates the EI concept.<sup>12</sup> Most convincingly, time-resolved photoemission spectroscopy reveals an extremely fast response of the CDW to external light pulses, which favors an electronic mechanism.<sup>13</sup> Alternatively, the coupling to the lattice degrees of freedom may drive the CDW transition, e.g., by a cooperative Jahn-Teller effect.<sup>14,15</sup> Here the particular form of the phonon dispersion and the softening of transverse optical phonon modes were elaborated within a tight-binding approach and found to agree with the experimental results.<sup>16–19</sup> The same holds for an *ab-initio* approach<sup>20</sup> to a Jahn-Teller effect. Likewise the onset of superconductivity by applying pressure may be understood within a phonon-driven CDW scenario.<sup>21</sup> Since some properties of the CDW in  $1T$ - $\text{TiSe}_2$  can be understood by the excitonic condensation of electron-hole pairs and others by the instability of a phonon mode, a combined scenario has been proposed.<sup>22</sup>

As yet it is unclear whether the chiral property of the CDW favors the electronic or lattice scenario, or a combination of both. In the present work, this issue is addressed amongst others. We start by investigating the CDW from an EI perspective. The corresponding mean-field approach for an extended Falicov-Kimball model is

presented in Sec. II A. We show that the EI scenario is insufficient to explain a stable chiral CDW. We proceed by including the lattice degrees of freedom. We find that the electron-phonon interaction and the phonon-phonon interaction both must be taken into account at least up to quartic order in the lattice distortion in order to stabilize chiral charge order. This is elaborated in Sec. II B, and in Sec. II C we present the ground-state energy as a function of the static lattice distortion. In Sec. II D the CDW phase boundary is derived. The CDW state is characterized analytically in Sec. II E. Section III contains our numerical results. Here we give the functional dependences of the relevant phases on the lattice distortion, show the finite-temperature phase diagram, derive the ground-state phase diagram, and estimate the interaction constants for  $1T$ - $\text{TiSe}_2$ . In Sec. IV, we summarize and conclude.

## II. MODEL AND THEORETICAL APPROACH

### A. Electronic degrees of freedom

#### 1. Band structure

Since the electronic properties of  $1T$ - $\text{TiSe}_2$  are dominated by the electrons near the Fermi energy, in what follows we take into account only the top valence band and the lower conduction band. The maximum of the valence band is located at the  $\Gamma$ -point. The conduction band exhibits minima at the three  $L$ -points, see Fig. 2. To facilitate the notation, we artificially split the conduc-

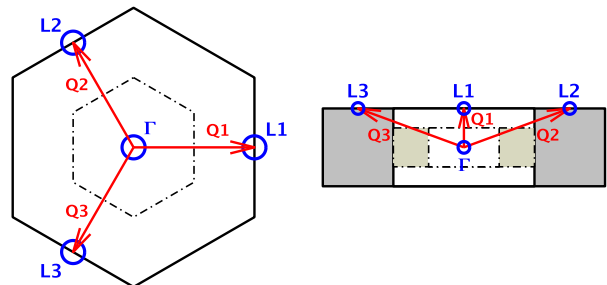


FIG. 2. (color online) First Brillouin zone (BZ) of  $1T$ - $\text{TiSe}_2$  with high-symmetry points in the normal phase (solid line) and in the CDW phase (dot-dashed line). Red arrows show the CDW ordering vectors. Left panel: projection onto the  $xy$ -plane, right panel: projection onto the  $yz$ -plane.

tion band into three symmetry-equivalent bands indexed by  $\alpha$ , each having one minimum at the point  $L_\alpha$ . The band dispersions of these three conduction bands mimics the true band structure close to the  $L$ -points.<sup>10</sup> Figure 3 illustrates the situation close to the Fermi level. Then

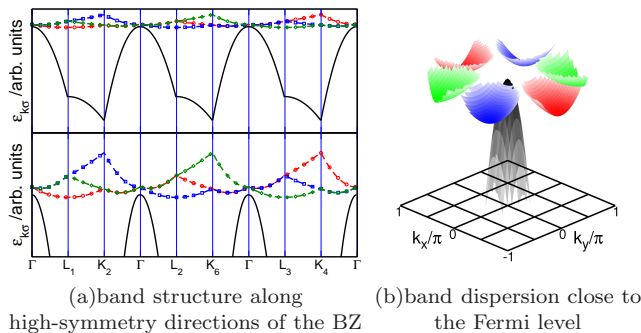


FIG. 3. (color online) Model band structure in the normal phase. The valence band is colored black, and the conduction bands are colored red, blue, and green.

158  
159 the free electron part is written as

$$H_e = \sum_{\mathbf{k}} \varepsilon_{\mathbf{k}f} f_{\mathbf{k}}^\dagger f_{\mathbf{k}} + \sum_{\mathbf{k}, \alpha} \varepsilon_{\mathbf{k}\alpha} c_{\mathbf{k}\alpha}^\dagger c_{\mathbf{k}\alpha}, \quad (2)$$

160 where  $f_{\mathbf{k}}^{(\dagger)}$  annihilates (creates) an electron in the valence  
161 band with momentum  $\mathbf{k}$  and  $c_{\mathbf{k}\alpha}^{(\dagger)}$  annihilates (creates) an  
162 electron in the conduction band with momentum  $\mathbf{k}$  and  
163 band index  $\alpha$ . The corresponding valence-band disper-  
164 sion and the conduction-band dispersions are denoted as  
165  $\varepsilon_{\mathbf{k}f}$  and  $\varepsilon_{\mathbf{k}\alpha}$ . They will be specified in Sec. III A. The  
166 spin of the electrons is neglected.

167 Taking the band structure and a band filling factor  
168  $n = 1/4$  into account, 1T-TiSe<sub>2</sub> resides in the vicinity of  
169 a semimetal-semiconductor transition, cf. Fig 3. Accord-  
170 ingly the chemical potential  $\mu$  is determined by

$$n_f + \sum_{\alpha} n_{\alpha} = 1, \quad (3)$$

171 where

$$n_f = \frac{1}{N} \sum_{\mathbf{k}} \langle n_{\mathbf{k}}^f \rangle = \frac{1}{N} \sum_{\mathbf{k}} \langle f_{\mathbf{k}}^\dagger f_{\mathbf{k}} \rangle, \quad (4)$$

$$n_{\alpha} = \frac{1}{N} \sum_{\mathbf{k}} \langle n_{\mathbf{k}}^{\alpha} \rangle = \frac{1}{N} \sum_{\mathbf{k}} \langle c_{\mathbf{k}\alpha}^\dagger c_{\mathbf{k}\alpha} \rangle. \quad (5)$$

172 Here  $N$  denotes the total number of lattice sites.

173 Regarding the isotropy (anisotropy) of the valence  
174 (conduction) band(s) the Fermi surface of 1T-TiSe<sub>2</sub> is  
175 only poorly nested,<sup>15</sup> which rules out a nesting mech-  
176 anism for the CDW formation even in a simplified 2D  
177 setting.

## 178 2. Electron-electron interaction

179 Due to the strong screening of the Coulomb interac-  
180 tion in 1T-TiSe<sub>2</sub>,<sup>23</sup> we assume a local electron-electron

181 interaction,

$$H_{e-e} = \frac{U_{cc}}{N} \sum_{\mathbf{k}, \mathbf{k}', \mathbf{q}} \sum_{\alpha} \sum_{\beta > \alpha} c_{\mathbf{k}+\mathbf{q}\alpha}^\dagger c_{\mathbf{k}\alpha} c_{\mathbf{k}'\beta}^\dagger c_{\mathbf{k}'+\mathbf{q}\beta} + \frac{U_{fc}}{N} \sum_{\mathbf{k}, \mathbf{k}', \mathbf{q}} \sum_{\alpha} f_{\mathbf{k}+\mathbf{q}}^\dagger f_{\mathbf{k}} c_{\mathbf{k}'\alpha}^\dagger c_{\mathbf{k}'+\mathbf{q}\alpha}, \quad (6)$$

182 where  $U_{cc}$  denotes the Coulomb repulsion among the con-  
183 duction electrons. The on-site Coulomb interaction  $U_{fc}$   
184 between valence and conduction band electrons deter-  
185 mines the distribution of electrons between these “sub-  
186 systems” and therefore may drive a valence transition, as  
187 observed, e.g., in heavy fermion and intermediate-valence  
188 Tm[Se,Te] compounds.<sup>24,25</sup> If the total electronic model  
189 contains an explicit hybridization between  $f$  and  $c$  elec-  
190 trons<sup>26,27</sup> or, as in our case, dispersive  $c$  and  $f$  bands,<sup>28</sup>  
191 coherence between  $c$  and  $f$  particles can develop. Then  
192  $U_{fc}$  may lead to a pairing of  $c$ -band electrons and  $f$ -band  
193 holes, i.e., to the formation of excitons, and, provided a  
194 large enough number of excitons is created, a subsequent  
195 spontaneous condensation of these composite quasipar-  
196 ticles may develop. In real systems this excitonic insta-  
197 bility is expected to occur, when semimetals with very  
198 small band overlap or semiconductors with very small  
199 band gap are cooled to extremely low temperatures.<sup>29,30</sup>  
200 The excitonic condensate then typifies a macroscopic  
201 phase-coherent insulating state, the EI, which separates  
202 the semimetal from the insulator.<sup>31,32</sup> From a theoretical  
203 point of view, Falicov-Kimball-type models seem to be  
204 the most promising candidates for realizing collective ex-  
205 citon phases. This holds particularly for the generic two-  
206 band extended Falicov-Kimball model (EFKM), where  
207 an EI ground state has been proven to exist in 1D and 2D  
208 by constrained-path Monte Carlo simulations.<sup>28,33</sup> Sub-  
209 sequent Hartree-Fock, slave-boson and projector-based  
210 renormalization techniques yield the 2D EFKM ground-  
211 state phase diagram in even quantitative accordance with  
212 unbiased Monte Carlo data,<sup>33–42</sup> supporting the applica-  
213 bility of these analytical approaches also in 3D and for  
214 more complicated situations.

215 The electronic part of our Hamiltonian,

$$H_{\text{mEFKM}} = H_e + H_{e-e}, \quad (7)$$

216 can be viewed as a multiband extended Falicov-Kimball  
217 model (mEFKM). We note that the mEFKM was studied  
218 previously and has been shown to reproduce the angle-  
219 resolved photoemission spectroscopy data for 1T-TiSe<sub>2</sub>  
220 at temperatures below the critical temperature,<sup>9,10,43–45</sup>  
221 as well as above but close to the critical temperature.<sup>23,46</sup>  
222 We note that the mEFKM exhibits a particular U(1)  
223 symmetry. This can be seen by applying the unitary  
224 transformation  $U_{\varphi, \alpha} = e^{i\varphi S_{\alpha}}$  with  $S_{\alpha} = \frac{1}{2} \sum_i (f_i^\dagger f_i -$   
225  $c_{i\alpha}^\dagger c_{i\alpha})$ . The operators  $f_i^{(\dagger)}$  and  $c_{i\alpha}^{(\dagger)}$  annihilate (create)  
226 an electron at Wannier site  $i$ . Obviously we have

$$H_{\text{mEFKM}} = U_{\varphi, \alpha} H_{\text{mEFKM}} U_{\varphi, \alpha}^\dagger. \quad (8)$$

227 This symmetry leads to a degeneracy between chiral and  
228 nonchiral CDWs (see below).

To proceed, we perform a Hartree-Fock decoupling of the electron-electron interaction terms:

$$\begin{aligned} & \frac{U_{cc}}{N} \sum_{\mathbf{k}, \mathbf{k}', \mathbf{q}} \sum_{\alpha} \sum_{\beta > \alpha} c_{\mathbf{k}+\mathbf{q}\alpha}^{\dagger} c_{\mathbf{k}\alpha} c_{\mathbf{k}'\beta}^{\dagger} c_{\mathbf{k}'+\mathbf{q}\beta} \rightarrow \\ & U_{cc} \sum_{\mathbf{k}} \sum_{\alpha} \sum_{\beta \neq \alpha} c_{\mathbf{k}\alpha}^{\dagger} c_{\mathbf{k}\alpha} n_{\beta} - NU_{cc} \sum_{\alpha} \sum_{\beta > \alpha} n_{\alpha} n_{\beta}, \end{aligned} \quad (9)$$

$$\begin{aligned} & \frac{U_{fc}}{N} \sum_{\mathbf{k}, \mathbf{k}', \mathbf{q}} \sum_{\alpha} f_{\mathbf{k}+\mathbf{q}\alpha}^{\dagger} f_{\mathbf{k}\alpha} c_{\mathbf{k}'\alpha}^{\dagger} c_{\mathbf{k}'+\mathbf{q}\alpha} \rightarrow \\ & U_{fc} \sum_{\alpha} n_{\alpha} \sum_{\mathbf{k}} f_{\mathbf{k}}^{\dagger} f_{\mathbf{k}} + U_{fc} n_f \sum_{\mathbf{k}, \alpha} c_{\mathbf{k}\alpha}^{\dagger} c_{\mathbf{k}\alpha} \\ & - NU_{fc} n_f \sum_{\alpha} n_{\alpha} - \sum_{\alpha} \Delta_{\mathbf{Q}\alpha} \sum_{\mathbf{k}} c_{\mathbf{k}+\mathbf{Q}\alpha}^{\dagger} f_{\mathbf{k}} \\ & - \sum_{\alpha} \Delta_{\mathbf{Q}\alpha}^* \sum_{\mathbf{k}} f_{\mathbf{k}}^{\dagger} c_{\mathbf{k}+\mathbf{Q}\alpha} + \frac{N}{U_{fc}} \sum_{\alpha} |\Delta_{\mathbf{Q}\alpha}|^2. \end{aligned} \quad (10)$$

Here we introduced the EI order parameter functions

$$\Delta_{\mathbf{Q}\alpha} = \frac{U_{fc}}{N} \sum_{\mathbf{k}} \langle f_{\mathbf{k}}^{\dagger} c_{\mathbf{k}+\mathbf{Q}\alpha} \rangle, \quad (11)$$

$$\Delta_{\mathbf{Q}\alpha}^* = \frac{U_{fc}}{N} \sum_{\mathbf{k}} \langle c_{\mathbf{k}+\mathbf{Q}\alpha}^{\dagger} f_{\mathbf{k}} \rangle. \quad (12)$$

Since the experiments on 1T-TiSe<sub>2</sub> suggest that the spontaneous hybridization of the valence band with one of the three conduction bands is the dominant effect of the electron-electron interaction,<sup>9</sup> in deriving Eq. (9), we neglected all terms that mix different conduction bands.

The resulting decoupled Hamiltonian takes the form

$$\begin{aligned} \bar{H}_{\text{mEFKM}} = & \sum_{\mathbf{k}} \bar{\epsilon}_{\mathbf{k}f} f_{\mathbf{k}}^{\dagger} f_{\mathbf{k}} + \sum_{\mathbf{k}, \alpha} \bar{\epsilon}_{\mathbf{k}\alpha} c_{\mathbf{k}\alpha}^{\dagger} c_{\mathbf{k}\alpha} \\ & - \sum_{\mathbf{k}, \alpha} \Delta_{\mathbf{Q}\alpha} c_{\mathbf{k}+\mathbf{Q}\alpha}^{\dagger} f_{\mathbf{k}} - \sum_{\mathbf{k}, \alpha} \Delta_{\mathbf{Q}\alpha}^* f_{\mathbf{k}}^{\dagger} c_{\mathbf{k}+\mathbf{Q}\alpha} \\ & - NU_{fc} n_f \sum_{\alpha} n_{\alpha} - NU_{cc} \sum_{\alpha} \sum_{\beta > \alpha} n_{\alpha} n_{\beta} \\ & + \frac{N}{U_{fc}} \sum_{\alpha} |\Delta_{\mathbf{Q}\alpha}|^2, \end{aligned} \quad (13)$$

with shifted  $f$ - and  $c$ -band dispersions:

$$\bar{\epsilon}_{\mathbf{k}f} = \epsilon_{\mathbf{k}f} + U_{fc} \sum_{\alpha} n_{\alpha}, \quad (14)$$

$$\bar{\epsilon}_{\mathbf{k}\alpha} = \epsilon_{\mathbf{k}\alpha} + U_{fc} n_f + U_{cc} \sum_{\beta \neq \alpha} n_{\beta}. \quad (15)$$

The EI low-temperature phase is characterized by non-vanishing expectation values  $\langle f_{\mathbf{k}}^{\dagger} c_{\mathbf{k}+\mathbf{Q}\alpha} \rangle$ ,  $\langle c_{\mathbf{k}+\mathbf{Q}\alpha}^{\dagger} f_{\mathbf{k}} \rangle$ , which cause a correlation gap in the excitation spectrum. The mean local electron density in the EI phase is

$$n_i = 1 + \frac{2}{N} \sum_{\mathbf{k}, \alpha} |\langle c_{\mathbf{k}+\mathbf{Q}\alpha}^{\dagger} f_{\mathbf{k}} \rangle| \cos(\mathbf{Q}_{\alpha} \mathbf{R}_i + \theta_{\alpha}), \quad (16)$$

$$\frac{1}{N} \sum_{\mathbf{k}} \langle c_{\mathbf{k}+\mathbf{Q}\alpha}^{\dagger} f_{\mathbf{k}} \rangle = \frac{1}{N} \sum_{\mathbf{k}} |\langle c_{\mathbf{k}+\mathbf{Q}\alpha}^{\dagger} f_{\mathbf{k}} \rangle| e^{i\theta_{\alpha}} = \frac{\Delta_{\mathbf{Q}\alpha}^*}{U_{fc}}. \quad (17)$$

Comparing Eq. (16) with relation (1) we recognize the amplitude of the charge density modulation as the modulus of the hybridization function  $\sum_{\mathbf{k}} \langle c_{\mathbf{k}+\mathbf{Q}\alpha}^{\dagger} f_{\mathbf{k}} \rangle$ . Likewise we can identify the initial phases  $\theta_{\alpha}$  in the density modulation as the phases of the hybridization functions (which coincide with the phases of the EI order parameters).

Note that previous theoretical studies of the mEFKM<sup>10,11</sup> did not include the phase differences of the  $\theta_{\alpha}$ , which will be essential for the establishment of a chiral CDW.<sup>5-8</sup> If one is not concerned with the chiral CDW problem, disregarding the phases  $\theta_{\alpha}$  seems to be justified since the U(1) symmetry of the mEFKM prevents the appearance of a stable chiral CDW anyway. We show this by analyzing the behavior of the electron operators under the unitary transformation  $U_{\varphi, \alpha}$ :  $c_{i\alpha}^{(\dagger)} = U_{\varphi, \alpha} c_{i\alpha}^{(\dagger)} U_{\varphi, \alpha}^{\dagger}$  and  $f_i^{(\dagger)} = U_{\varphi, \alpha} f_i^{(\dagger)} U_{\varphi, \alpha}^{\dagger}$ . The hybridization functions (in real space) then transform as  $\langle c_{i\alpha}^{\dagger} f_i \rangle e^{i\mathbf{Q}_{\alpha} \mathbf{R}_i} = e^{-i\varphi} \langle \tilde{c}_{i\alpha}^{\dagger} \tilde{f}_i \rangle e^{i\mathbf{Q}_{\alpha} \mathbf{R}_i}$ . That is, the phases  $\theta_{\alpha}$  can be controlled by the unitary transformation through the angles  $\varphi$ . However, in view of (8) the total energy is independent of the  $\theta_{\alpha}$ . Hence these phases can be chosen arbitrarily, and there is no mechanism that stabilizes a given phase difference. Therefore the mEFKM is insufficient to describe a chiral CDW in 1T-TiSe<sub>2</sub>. In the following we will demonstrate that the coupling of the electrons to the lattice degrees of freedom can break the U(1) symmetry of the mEFKM and consequently can stabilize a chiral CDW.

## B. Lattice degrees of freedom

### 1. Electron-phonon coupling

For 1T-TiSe<sub>2</sub> there are experimental and theoretical evidences that the weak periodic lattice distortion observed comes from a softening of a transverse optical phonon mode.<sup>16-20</sup> We therefore include a single-mode electron-phonon interaction in our model. If we expand the electron-lattice interaction up to quartic order in the lattice distortion, we obtain the electron-phonon interaction as

$$H_{e\text{-ph}} = H_{e\text{-ph}}^{(1)} + H_{e\text{-ph}}^{(2)} + H_{e\text{-ph}}^{(3)} + H_{e\text{-ph}}^{(4)}, \quad (18)$$

where

$$H_{e\text{-ph}}^{(1)} = \frac{1}{\sqrt{N}} \sum_{\mathbf{k}, \mathbf{q}} \sum_{\lambda, \lambda'} g_1(\mathbf{k}, \mathbf{q}, \lambda, \lambda') (b_{\mathbf{q}}^{\dagger} + b_{-\mathbf{q}}) c_{\mathbf{k}\lambda}^{\dagger} c_{\mathbf{k}+\mathbf{q}\lambda'}, \quad (19)$$

282

$$H_{e-ph}^{(2)} = \frac{1}{2N} \sum_{\mathbf{k}, \mathbf{q}_1, \mathbf{q}_2} \sum_{\lambda, \lambda'} g_2(\mathbf{k}, \mathbf{q}_1, \mathbf{q}_2, \lambda, \lambda') (b_{\mathbf{q}_1}^\dagger + b_{-\mathbf{q}_1}) \times (b_{\mathbf{q}_2}^\dagger + b_{-\mathbf{q}_2}) c_{\mathbf{k}\lambda}^\dagger c_{\mathbf{k}+\mathbf{q}_1+\mathbf{q}_2\lambda'}, \quad (20)$$

$$H_{e-ph}^{(3)} = \frac{1}{6N^{\frac{3}{2}}} \sum_{\mathbf{k}, \mathbf{q}_1, \mathbf{q}_2, \mathbf{q}_3} \sum_{\lambda, \lambda'} g_3(\mathbf{k}, \mathbf{q}_1, \mathbf{q}_2, \mathbf{q}_3, \lambda, \lambda') \times (b_{\mathbf{q}_1}^\dagger + b_{-\mathbf{q}_1}) (b_{\mathbf{q}_2}^\dagger + b_{-\mathbf{q}_2}) (b_{\mathbf{q}_3}^\dagger + b_{-\mathbf{q}_3}) \times c_{\mathbf{k}\lambda}^\dagger c_{\mathbf{k}+\mathbf{q}_1+\mathbf{q}_2+\mathbf{q}_3\lambda'}, \quad (21)$$

$$H_{e-ph}^{(4)} = \frac{1}{24N^2} \sum_{\mathbf{k}, \mathbf{q}_1, \mathbf{q}_2, \mathbf{q}_3, \mathbf{q}_4} \sum_{\lambda, \lambda'} g_4(\mathbf{k}, \mathbf{q}_1, \mathbf{q}_2, \mathbf{q}_3, \mathbf{q}_4, \lambda, \lambda') \times (b_{\mathbf{q}_1}^\dagger + b_{-\mathbf{q}_1}) (b_{\mathbf{q}_2}^\dagger + b_{-\mathbf{q}_2}) (b_{\mathbf{q}_3}^\dagger + b_{-\mathbf{q}_3}) \times (b_{\mathbf{q}_4}^\dagger + b_{-\mathbf{q}_4}) c_{\mathbf{k}\lambda}^\dagger c_{\mathbf{k}+\mathbf{q}_1+\mathbf{q}_2+\mathbf{q}_3+\mathbf{q}_4\lambda'}, \quad (22)$$

283 where  $b_{\mathbf{q}}^{(\dagger)}$  describes the annihilation (creation) operator  
284 of a phonon carrying the momentum  $\mathbf{q}$ ,  $g_i$  ( $i = 1, 2, 3, 4$ )  
285 denote the electron-phonon coupling constants, and  $\lambda$ ,  
286  $\lambda'$  label the band degree of freedom. Most notably the  
287 band-mixing terms; i.e., if  $\lambda \neq \lambda'$  in Eqs. (19)-(22), break  
288 the U(1) symmetry of the mEFKM, i.e., the arbitrariness  
289 with respect to the phases  $\theta_\alpha$  is eliminated.

290

## 2. Phonon-phonon interaction

291 Within the harmonic approximation, the Hamiltonian  
292 for the (noninteracting) phonons reads<sup>47</sup>

$$H_{\text{ph}} = \sum_{\mathbf{q}} \hbar\omega(\mathbf{q}) b_{\mathbf{q}}^\dagger b_{\mathbf{q}}, \quad (23)$$

293 where  $\omega(\mathbf{q})$  is the bare phonon frequency. A coupling be-  
294 tween the lattice vibrations results from the anharmonic  
295 contributions in the expansion of the potential for the  
296 ions.<sup>48</sup> As we will see below, such an explicit phonon-  
297 phonon interaction may stabilize the chiral CDW phase.  
298 We expand the phonon-phonon interaction also up to  
299 quartic order in the lattice displacement. We obtain

$$H_{\text{ph-ph}} = \frac{1}{\sqrt{N}} \sum_{\mathbf{q}_1, \mathbf{q}_2, \mathbf{q}_3} B(\mathbf{q}_1, \mathbf{q}_2, \mathbf{q}_3) (b_{\mathbf{q}_1}^\dagger + b_{-\mathbf{q}_1}) \times (b_{\mathbf{q}_2}^\dagger + b_{-\mathbf{q}_2}) (b_{\mathbf{q}_3}^\dagger + b_{-\mathbf{q}_3}) + \frac{1}{N} \sum_{\mathbf{q}_1, \mathbf{q}_2, \mathbf{q}_3, \mathbf{q}_4} D(\mathbf{q}_1, \mathbf{q}_2, \mathbf{q}_3, \mathbf{q}_4) (b_{\mathbf{q}_1}^\dagger + b_{-\mathbf{q}_1}) \times (b_{\mathbf{q}_2}^\dagger + b_{-\mathbf{q}_2}) (b_{\mathbf{q}_3}^\dagger + b_{-\mathbf{q}_3}) (b_{\mathbf{q}_4}^\dagger + b_{-\mathbf{q}_4}). \quad (24)$$

300 The explicit expressions of  $B(\mathbf{q}_1, \mathbf{q}_2, \mathbf{q}_3)$  and  
301  $D(\mathbf{q}_1, \mathbf{q}_2, \mathbf{q}_3, \mathbf{q}_4)$  are lengthy. We note only the  
302 symmetry relations

$$B(-\mathbf{q}_1, -\mathbf{q}_2, -\mathbf{q}_3) = B^*(\mathbf{q}_1, \mathbf{q}_2, \mathbf{q}_3), \quad (25)$$

$$D(-\mathbf{q}_1, -\mathbf{q}_2, -\mathbf{q}_3, -\mathbf{q}_4) = D^*(\mathbf{q}_1, \mathbf{q}_2, \mathbf{q}_3, \mathbf{q}_4), \quad (26)$$

303 and point out the constraints

$$B(\mathbf{q}_1, \mathbf{q}_2, \mathbf{q}_3) \propto \delta_{\mathbf{q}_1+\mathbf{q}_2+\mathbf{q}_3, \mathbf{G}}, \quad (27)$$

$$D(\mathbf{q}_1, \mathbf{q}_2, \mathbf{q}_3, \mathbf{q}_4) \propto \delta_{\mathbf{q}_1+\mathbf{q}_2+\mathbf{q}_3+\mathbf{q}_4, \mathbf{G}}. \quad (28)$$

304 Here  $\mathbf{G}$  is a reciprocal lattice vector of the undistorted  
305 lattice.

306

## 3. Frozen-phonon approach

307 We now apply the frozen-phonon approximation and  
308 calculate the lattice distortion at low temperatures. As  
309 elaborated in Refs. 17–20 the phonons causing the lat-  
310 tice displacements in 1T-TiSe<sub>2</sub> have the momenta  $\mathbf{Q}_\alpha$   
311 shown in Fig. 2. Their softening is inherently con-  
312 nected to strong electronic correlations.<sup>23</sup> It has been  
313 suggested that the  $\mathbf{Q}_1$ ,  $\mathbf{Q}_2$ , and  $\mathbf{Q}_3$  phonons become  
314 soft at the same temperature;<sup>18</sup> we therefore assume  
315  $|g_1(\mathbf{k}, \mathbf{Q}_1, \lambda, \lambda')| = |g_1(\mathbf{k}, \mathbf{Q}_2, \lambda, \lambda')| = |g_1(\mathbf{k}, \mathbf{Q}_3, \lambda, \lambda')| =$   
316  $g_{1\mathbf{Q}}(\mathbf{k})$ , likewise the other electron-phonon coupling con-  
317 stants, and  $\omega(\mathbf{Q}_1) = \omega(\mathbf{Q}_2) = \omega(\mathbf{Q}_3) = \omega$ . A finite  
318 displacement of the ions is characterized by  $\langle b_{\mathbf{Q}_\alpha}^\dagger \rangle =$   
319  $\langle b_{-\mathbf{Q}_\alpha} \rangle \neq 0$ . We denote the static lattice distortions by

$$\delta_{\mathbf{Q}_\alpha} = \frac{2}{\sqrt{N}} \langle b_{\mathbf{Q}_\alpha} \rangle = |\delta_{\mathbf{Q}_\alpha}| e^{-i\phi_\alpha}, \quad (29)$$

$$\delta_{\mathbf{Q}_\alpha}^* = \frac{2}{\sqrt{N}} \langle b_{\mathbf{Q}_\alpha}^\dagger \rangle = |\delta_{\mathbf{Q}_\alpha}| e^{i\phi_\alpha}. \quad (30)$$

320 Replacing all phonon operators by their averages, the  
321 Hamiltonian  $H = H_e + H_{e-e} + H_{e-ph} + H_{\text{ph}} + H_{\text{ph-ph}}$   
322 becomes an effective electronic model,

$$\begin{aligned} \bar{H} = & \sum_{\mathbf{k}, \alpha} g_{1\mathbf{Q}}(\mathbf{k}) (\delta_{\mathbf{Q}_\alpha} c_{\mathbf{k}+\mathbf{Q}_\alpha}^\dagger f_{\mathbf{k}} + \delta_{\mathbf{Q}_\alpha}^* f_{\mathbf{k}} c_{\mathbf{k}+\mathbf{Q}_\alpha}) \\ & + \frac{1}{2} \sum_{\mathbf{k}} \sum_{\alpha, \beta} [\bar{A}_{\mathbf{Q}}^f(\mathbf{k}) f_{\mathbf{k}}^\dagger f_{\mathbf{k}} + \bar{A}_{\mathbf{Q}}^c(\mathbf{k}) c_{\mathbf{k}\beta}^\dagger c_{\mathbf{k}\beta}] [(\delta_{\mathbf{Q}_\alpha}^*)^2 + \delta_{\mathbf{Q}_\alpha}^2] \\ & + \frac{1}{6} \sum_{\mathbf{k}} \sum_{\alpha, \beta} \{ \bar{B}_{1\mathbf{Q}}^{\alpha\beta}(\mathbf{k}) [(\delta_{\mathbf{Q}_\beta}^*)^2 + \delta_{\mathbf{Q}_\beta}^2] + \bar{B}_{2\mathbf{Q}}^{\alpha\beta}(\mathbf{k}) |\delta_{\mathbf{Q}_\beta}|^2 \} \\ & \times (\delta_{\mathbf{Q}_\alpha} c_{\mathbf{k}+\mathbf{Q}_\alpha}^\dagger f_{\mathbf{k}} + \delta_{\mathbf{Q}_\alpha}^* f_{\mathbf{k}} c_{\mathbf{k}+\mathbf{Q}_\alpha}) \\ & + \frac{1}{24} \sum_{\mathbf{k}} \sum_{\alpha, \gamma} \sum_{\beta \neq \alpha} \{ [\tilde{C}_{\alpha\beta}^f(\mathbf{k}) f_{\mathbf{k}}^\dagger f_{\mathbf{k}} + \tilde{C}_{\alpha\beta}^c(\mathbf{k}) c_{\mathbf{k}\gamma}^\dagger c_{\mathbf{k}\gamma}] \\ & \times [(\delta_{\mathbf{Q}_\alpha}^* \delta_{\mathbf{Q}_\beta}^*)^2 + (\delta_{\mathbf{Q}_\alpha}^* \delta_{\mathbf{Q}_\beta})^2] + [(\tilde{C}_{\alpha\beta}^f(\mathbf{k}))^* f_{\mathbf{k}}^\dagger f_{\mathbf{k}} \\ & + (\tilde{C}_{\alpha\beta}^c(\mathbf{k}))^* c_{\mathbf{k}\gamma}^\dagger c_{\mathbf{k}\gamma}] [(\delta_{\mathbf{Q}_\alpha} \delta_{\mathbf{Q}_\beta})^2 + (\delta_{\mathbf{Q}_\alpha} \delta_{\mathbf{Q}_\beta}^*)^2] \} \\ & + \hat{D}N \sum_{\alpha} \sum_{\beta > \alpha} [(\delta_{\mathbf{Q}_\alpha}^* \delta_{\mathbf{Q}_\beta}^*)^2 + (\delta_{\mathbf{Q}_\alpha} \delta_{\mathbf{Q}_\beta})^2 + (\delta_{\mathbf{Q}_\alpha}^* \delta_{\mathbf{Q}_\beta})^2 \\ & + (\delta_{\mathbf{Q}_\alpha} \delta_{\mathbf{Q}_\beta}^*)^2] + \tilde{D}N \sum_{\alpha} |\delta_{\mathbf{Q}_\alpha}|^4 + \frac{\hbar\omega}{4} N \sum_{\alpha} |\delta_{\mathbf{Q}_\alpha}|^2 \\ & + \bar{H}_{\text{mEFKM}}, \end{aligned} \quad (31)$$

323 where  $\alpha, \beta, \gamma = 1, 2, 3$ . Moreover, it is  $\hat{D} =$   
324  $2D(\mathbf{Q}_\alpha, \mathbf{Q}_\alpha, \mathbf{Q}_\beta, \mathbf{Q}_\beta)$ , where  $\beta \neq \alpha$ , and  $\tilde{D} =$

325  $D(\mathbf{Q}_\alpha, \mathbf{Q}_\alpha, \mathbf{Q}_\alpha, \mathbf{Q}_\alpha)$ . The electron-phonon and phonon-  
 326 phonon interaction constants are considered as real num-  
 327 bers except  $\tilde{C}_{\alpha\beta}^f(\mathbf{k})$  and  $\tilde{C}_{\alpha\beta}^c(\mathbf{k})$ . The phases of these  
 328 constants must be taken into account, otherwise chirality  
 329 will not develop in our model. For the electron-phonon  
 330 coupling constants we use the shorthand notation,

$$g_{1\mathbf{Q}}(\mathbf{k}) = g_1(\mathbf{k}, \mathbf{Q}_\alpha, f, \alpha), \quad (32)$$

$$\bar{A}_{1\mathbf{Q}}^f(\mathbf{k}) = g_2(\mathbf{k}, \mathbf{Q}_\alpha, \mathbf{Q}_\alpha, f, f), \quad (33)$$

$$\bar{A}_{1\mathbf{Q}}^c(\mathbf{k}) = g_2(\mathbf{k}, \mathbf{Q}_\alpha, \mathbf{Q}_\alpha, 1, 1), \quad (34)$$

$$\bar{B}_{1\mathbf{Q}}^{\alpha\beta}(\mathbf{k}) = 3g_3(\mathbf{k}, \mathbf{Q}_\beta, \mathbf{Q}_\beta, \mathbf{Q}_\alpha, f, \alpha), \quad (35)$$

$$\bar{B}_{2\mathbf{Q}}^{\alpha\beta}(\mathbf{k}) = 6g_3(\mathbf{k}, \mathbf{Q}_\beta, -\mathbf{Q}_\beta, \mathbf{Q}_\alpha, f, \alpha), \quad (36)$$

$$\tilde{C}_{\alpha\beta}^f(\mathbf{k}) = 6g_4(\mathbf{k}, \mathbf{Q}_\alpha, \mathbf{Q}_\alpha, \mathbf{Q}_\beta, \mathbf{Q}_\beta, f, f), \quad (37)$$

$$\tilde{C}_{\alpha\beta}^c(\mathbf{k}) = 6g_4(\mathbf{k}, \mathbf{Q}_\alpha, \mathbf{Q}_\alpha, \mathbf{Q}_\beta, \mathbf{Q}_\beta, 1, 1). \quad (38)$$

331 We assume for simplicity that the phonon-phonon in-  
 332 teraction constants are the same for all combinations of  $\alpha$   
 333 and  $\beta$ . In Eq. (31), the term proportional to  $\tilde{D}$ , coming  
 334 from the expansion of the phonon-phonon interaction,  
 335 guarantees that the free energy is bounded from below  
 336 within our approximations. Obviously, a finite lattice dis-  
 337 tortion causes a hybridization between the valence and  
 338 the conduction bands. As a consequence a gap in the  
 339 electronic spectrum opens, just as in the course of exci-  
 340 ton condensation [cf. Eq. (13)]. The corresponding local  
 341 electron density is given by Eq. (16).

342 Of particular interest are the phases  $\theta_\alpha$ . Owing to the  
 343 terms on the r.h.s. of Eq. (31) proportional to  $g_{1\mathbf{Q}}(\mathbf{k})$   
 344 and  $\bar{B}_{i\mathbf{Q}}^{\alpha\beta}(\mathbf{k})$ , these phases are coupled to the phases of  
 345  $\delta_{\mathbf{Q}_\alpha}$ . Let us analyze the possible values of the phases of  
 346 the static lattice distortion. We first note that every  $\mathbf{Q}_\alpha$   
 347 is half a reciprocal lattice vector in the normal phase,  
 348 i.e.,  $e^{2i\mathbf{Q}_\alpha \cdot \mathbf{R}_i} = 1$ , where  $\mathbf{R}_i$  is a lattice vector of the  
 349 undistorted lattice. Hence

$$\begin{aligned} b_{\mathbf{Q}_\alpha}^\dagger &= \frac{1}{\sqrt{N}} \sum_i b_i^\dagger e^{-i\mathbf{Q}_\alpha \cdot \mathbf{R}_i} = \frac{1}{\sqrt{N}} \sum_i b_i^\dagger e^{-i\mathbf{Q}_\alpha \cdot \mathbf{R}_i + 2i\mathbf{Q}_\alpha \cdot \mathbf{R}_i} \\ &= \frac{1}{\sqrt{N}} \sum_i b_i^\dagger e^{i\mathbf{Q}_\alpha \cdot \mathbf{R}_i} = b_{-\mathbf{Q}_\alpha}^\dagger. \end{aligned} \quad (39)$$

350 That is,  $b_{\mathbf{Q}_\alpha}^\dagger$  and  $b_{-\mathbf{Q}_\alpha}^\dagger$  create the same phonon. This im-  
 351 plies  $\langle b_{\mathbf{Q}_\alpha}^\dagger \rangle = \langle b_{-\mathbf{Q}_\alpha}^\dagger \rangle = \langle b_{\mathbf{Q}_\alpha} \rangle$ . Consequently,  $\langle b_{\mathbf{Q}_\alpha} \rangle$  and  
 352  $\delta_{\mathbf{Q}_\alpha}$  become real numbers. However, since a triple CDW  
 353 is not a simple superposition of three single CDWs, the  
 354 situation is more subtle. Here, the change of the period-  
 355 icity of the lattice caused by one CDW component affects  
 356 the formation of the other two components. To elucidate  
 357 this in more detail let us assume that phonon 1 softens  
 358 at  $T_c$ , while phonon 2 and phonon 3 soften at  $T_c - \delta T$ .  
 359 As a result of the transition 1 at  $T_c$  the periodicity of  
 360 the crystal changes and consequently the BZ changes too  
 361 (cf. Fig. 4). The vectors  $\mathbf{Q}_2$  and  $\mathbf{Q}_3$  are no longer half-  
 362 reciprocal lattice vectors, and Eq. (39) does not apply.  
 363 Hence, at  $T_c - \delta T$ ,  $\langle b_{\mathbf{Q}_2} \rangle$  and  $\langle b_{\mathbf{Q}_3} \rangle$  are complex numbers  
 364 with phases that have to be determined by minimizing

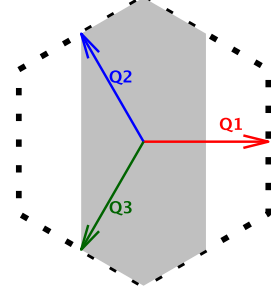


FIG. 4. (color online) BZ in the normal phase (black dotted hexagon) and (artificial) BZ that would emerge if only the phonon  $\mathbf{Q}_1$  softens (filled gray hexagon). Red, green, and blue arrows indicate the ordering vectors  $\mathbf{Q}_1$ ,  $\mathbf{Q}_2$ , and  $\mathbf{Q}_3$ , respectively.

366 the free energy. For  $1T$ -TiSe<sub>2</sub>,  $\delta T = 0$ , but nevertheless  
 367 the above discussion remains valid. That is the freedom  
 368 to fix the phases of the lattice distortions in an appro-  
 369 priate way results from the fact that one triple-CDW  
 370 component must develop in a lattice structure which is  
 371 already distorted by the other two triple-CDW compo-  
 372 nents.

### C. Ground-state energy

Based on the model (31) we analyze the chiral CDW  
 formation at zero temperature. Taking into account the  
 symmetry of the conduction bands and the equality of the  
 interaction constants, we have  $|\delta_{\mathbf{Q}_1}| = |\delta_{\mathbf{Q}_2}| = |\delta_{\mathbf{Q}_3}| = |\delta_{\mathbf{Q}}|$   
 and  $|\Delta_{\mathbf{Q}_1}| = |\Delta_{\mathbf{Q}_2}| = |\Delta_{\mathbf{Q}_3}| = |\Delta_{\mathbf{Q}}|$ . Therewith the  
 ground-state energy per site follows as

$$\begin{aligned} \frac{\bar{E}}{N} &= \frac{2}{N} \sum_{\mathbf{k}, \alpha} g_{1\mathbf{Q}}(\mathbf{k}) |\delta_{\mathbf{Q}}| |\langle c_{\mathbf{k}+\mathbf{Q}_\alpha}^\dagger f_{\mathbf{k}} \rangle| \cos(\phi_\alpha - \theta_\alpha) \\ &+ \frac{1}{N} \sum_{\mathbf{k}} \sum_{\alpha, \beta} |\delta_{\mathbf{Q}}|^2 [\bar{A}_{\mathbf{Q}}^f(\mathbf{k}) \langle f_{\mathbf{k}}^\dagger f_{\mathbf{k}} \rangle + \bar{A}_{\mathbf{Q}}^c(\mathbf{k}) \langle c_{\mathbf{k}\beta}^\dagger c_{\mathbf{k}\beta} \rangle] \\ &\times \cos(2\phi_\alpha) + \frac{1}{3N} \sum_{\mathbf{k}} \sum_{\alpha, \beta} |\delta_{\mathbf{Q}}|^3 |\langle c_{\mathbf{k}+\mathbf{Q}_\alpha}^\dagger f_{\mathbf{k}} \rangle| \\ &\times [2\bar{B}_{1\mathbf{Q}}^{\alpha\beta}(\mathbf{k}) \cos(2\phi_\beta) + \bar{B}_{2\mathbf{Q}}^{\alpha\beta}(\mathbf{k}) \cos(\phi_\alpha - \theta_\alpha)] \\ &+ \frac{1}{12N} \sum_{\mathbf{k}} \sum_{\alpha, \gamma} \sum_{\beta \neq \alpha} [\bar{C}_{\alpha\beta}^f(\mathbf{k}) \langle f_{\mathbf{k}}^\dagger f_{\mathbf{k}} \rangle + \bar{C}_{\alpha\beta}^c(\mathbf{k}) \langle c_{\mathbf{k}\gamma}^\dagger c_{\mathbf{k}\gamma} \rangle] \\ &\times |\delta_{\mathbf{Q}}|^4 [\cos(2(\phi_\alpha - \phi_\beta) + \phi_C) + \cos(2(\phi_\alpha + \phi_\beta) + \phi_C)] \\ &+ 4\hat{D} \sum_{\alpha} \sum_{\beta > \alpha} |\delta_{\mathbf{Q}}|^4 \cos(2\phi_\alpha) \cos(2\phi_\beta) + 3\tilde{D} |\delta_{\mathbf{Q}}|^4 \\ &+ \frac{3}{4} \hbar \omega |\delta_{\mathbf{Q}}|^2 + \frac{\bar{E}_{\text{mEFKM}}}{N}, \end{aligned} \quad (40)$$

374 where  $\tilde{C}_{\alpha\beta}^{f(c)} = \bar{C}_{\alpha\beta}^{f(c)} e^{-i\phi_C}$ . We note that each phase  
 375  $\theta_\alpha$  is exclusively coupled to  $\phi_\alpha$ . If  $\sum_{\mathbf{k}} [g_{1\mathbf{Q}}(\mathbf{k}) +$

376  $\sum_{\beta} (2\bar{B}_{1\mathbf{Q}}^{\alpha\beta}(\mathbf{k}) \cos(2\phi_{\beta}) + \bar{B}_{2\mathbf{Q}}^{\alpha\beta}(\mathbf{k}) |\delta_{\mathbf{Q}\beta}|^2) |\langle c_{\mathbf{k}+\mathbf{Q}\alpha}^{\dagger} f_{\mathbf{k}} \rangle| >$   
 377 0, the choice

$$\theta_{\alpha} = \phi_{\alpha} + (2s + 1)\pi, \quad (41)$$

378 minimizes the energy, where  $s = 0, 1, 2, \dots$ . Otherwise  $\theta_{\alpha}$   
 379 are locked to  $\phi_{\alpha} + 2s\pi$ . Thus, the relationship between  
 380  $\phi_1, \phi_2$ , and  $\phi_3$  is crucial.

381 The Hamiltonian (31) offers a complex model with  
 382 many (unknown) parameters. To proceed we assume the  
 383 electron-phonon interaction constants as independent of  
 384 the momentum  $\mathbf{k}$ . Moreover, we assume that  $\bar{A}_{\mathbf{Q}}^f, \bar{A}_{\mathbf{Q}}^c,$   
 385  $\bar{B}_{1\mathbf{Q}}^{\alpha\beta}, \bar{B}_{2\mathbf{Q}}^{\alpha\beta}, \bar{C}_{\alpha\beta}^f, \bar{C}_{\alpha\beta}^c, \hat{D}$ , and  $\tilde{D}$  are much smaller than  
 386  $U_{fc}, U_{cc}$ , and  $g_{1\mathbf{Q}}$ . The magnitude of the EI order param-  
 387 eter and the static lattice distortion are then primarily  
 388 determined by the latter interaction constants and the  
 389 constraint for Eq. (41) simply reduces to  $g_{1\mathbf{Q}} > 0$ . Tak-  
 390 ing only  $U_{fc}, U_{cc}$ , and  $g_{1\mathbf{Q}}$  into account and minimizing  
 391 the free energy with respect to the EI order parameter  
 392 yields  $\frac{\partial F}{\partial |\Delta_{\mathbf{Q}}|} = \frac{\partial F}{\partial |\Delta_{\mathbf{Q}}|} + \frac{6}{U_{fc}} |\Delta_{\mathbf{Q}}| = 0$ , while the minimiza-  
 393 tion with respect to the static lattice distortion yields  
 394  $\frac{\partial F}{\partial |\delta_{\mathbf{Q}}|} = g_{1\mathbf{Q}} \frac{\partial F}{\partial |\Delta_{\mathbf{Q}}|} + \frac{6}{4} \hbar\omega |\delta_{\mathbf{Q}}| = 0$ , where the gap param-  
 395 eter is given by

$$\tilde{\Delta}_{\mathbf{Q}\alpha} = g_{1\mathbf{Q}} \delta_{\mathbf{Q}\alpha} - \Delta_{\mathbf{Q}\alpha}. \quad (42)$$

396 The relation (41) maximizes the modulus of the gap pa-  
 397 rameter (supposing  $g_{1\mathbf{Q}} > 0$ ). From the energy mini-  
 398 mization with respect to  $|\Delta_{\mathbf{Q}}|$  and  $|\delta_{\mathbf{Q}}|$

$$|\Delta_{\mathbf{Q}}| = \frac{U_{fc} \hbar\omega}{4 g_{1\mathbf{Q}}} |\delta_{\mathbf{Q}}|. \quad (43)$$

399 With Eqs. (41) and (43) we can express the ground-state  
 400 energy per site as

$$\frac{\bar{E}}{N} = \frac{1}{N} \bar{E}_{\delta} (|\delta_{\mathbf{Q}}|^2) + \frac{1}{N} \bar{E}_{\phi} (|\delta_{\mathbf{Q}}|^2, \phi_1, \phi_2, \phi_3), \quad (44)$$

where

$$\begin{aligned} \frac{1}{N} \bar{E}_{\delta} (|\delta_{\mathbf{Q}}|^2) &= \frac{1}{N} \sum_{\mathbf{k}, \nu} E_{\mathbf{k}\nu} \langle n_{\mathbf{k}}^{\nu} \rangle - U_{fc} n_f (1 - n_f) \\ &- \frac{U_{cc}}{3} (1 - n_f)^2 + \frac{3}{4} \hbar\omega |\delta_{\mathbf{Q}}|^2 + \frac{3}{16} U_{fc} \left( \frac{\hbar\omega}{g_{1\mathbf{Q}}} \right)^2 |\delta_{\mathbf{Q}}|^2 \\ &+ \left( 3\tilde{D} - \frac{1}{12} \hat{B}_{2\mathbf{Q}} \frac{\hbar\omega}{g_{1\mathbf{Q}}} \right) |\delta_{\mathbf{Q}}|^4, \quad (45) \\ \frac{1}{N} \bar{E}_{\phi} (|\delta_{\mathbf{Q}}|^2, \phi_1, \phi_2, \phi_3) &= [\bar{A}_{\mathbf{Q}}^f n_f + \bar{A}_{\mathbf{Q}}^c (1 - n_f)] |\delta_{\mathbf{Q}}|^2 \\ &\times \sum_{\alpha} \cos(2\phi_{\alpha}) - \frac{1}{6} \frac{\hbar\omega}{g_{1\mathbf{Q}}} |\delta_{\mathbf{Q}}|^4 \sum_{\alpha} \hat{B}_{1\mathbf{Q}}^{\alpha} \cos(2\phi_{\alpha}) \\ &+ \frac{1}{12} \sum_{\alpha} \sum_{\beta \neq \alpha} [\bar{C}_{\alpha\beta}^f n_f + \bar{C}_{\alpha\beta}^c (1 - n_f)] |\delta_{\mathbf{Q}}|^4 \\ &\times [\cos(2(\phi_{\alpha} - \phi_{\beta}) + \phi_C) + \cos(2(\phi_{\alpha} + \phi_{\beta}) + \phi_C)] \\ &+ 4\hat{D} |\delta_{\mathbf{Q}}|^4 \sum_{\alpha} \sum_{\beta > \alpha} \cos(2\phi_{\alpha}) \cos(2\phi_{\beta}). \quad (46) \end{aligned}$$

401 Here,  $\hat{B}_{2\mathbf{Q}} = \sum_{\alpha, \beta} \bar{B}_{2\mathbf{Q}}^{\alpha\beta}$  and  $\hat{B}_{1\mathbf{Q}}^{\alpha} = \sum_{\beta} \bar{B}_{1\mathbf{Q}}^{\beta\alpha}$ . The quasi-  
 402 particle energies  $E_{\mathbf{k}\nu}$  ( $\nu = A, B, C, D$ ) are obtained by  
 403 the diagonalization of the Hamilton matrix

$$[H] = \begin{pmatrix} \bar{\epsilon}_{\mathbf{k}f} & \tilde{\Delta}_{\mathbf{Q}1}^* & \tilde{\Delta}_{\mathbf{Q}2}^* & \tilde{\Delta}_{\mathbf{Q}3}^* \\ \tilde{\Delta}_{\mathbf{Q}1} & \bar{\epsilon}_{\mathbf{k}+\mathbf{Q}1} & 0 & 0 \\ \tilde{\Delta}_{\mathbf{Q}2} & 0 & \bar{\epsilon}_{\mathbf{k}+\mathbf{Q}2} & 0 \\ \tilde{\Delta}_{\mathbf{Q}3} & 0 & 0 & \bar{\epsilon}_{\mathbf{k}+\mathbf{Q}3} \end{pmatrix}. \quad (47)$$

404 Since only  $|\tilde{\Delta}_{\mathbf{Q}}|^2$  enters  $E_{\mathbf{k}\nu}$  we may replace  $\tilde{\Delta}_{\mathbf{Q}\alpha}$  by

$$|\tilde{\Delta}_{\mathbf{Q}}| = \left( g_{1\mathbf{Q}} + \frac{U_{fc} \hbar\omega}{4 g_{1\mathbf{Q}}} \right) |\delta_{\mathbf{Q}}| \quad (48)$$

405 in Eq. (47). The choice

$$\begin{aligned} \tilde{D} \geq 4\hat{D} + \frac{1}{3} \sum_{\alpha} \sum_{\beta > \alpha} (\bar{C}_{\alpha\beta}^f + \bar{C}_{\alpha\beta}^c) + \frac{1}{6} \sum_{\alpha} \hat{B}_{1\mathbf{Q}}^{\alpha} \frac{\hbar\omega}{g_{1\mathbf{Q}}} \\ + \frac{1}{12} B_{2\mathbf{Q}} \frac{\hbar\omega}{g_{1\mathbf{Q}}} \quad (49) \end{aligned}$$

406 guarantees the lower boundary of the energy. In the nu-  
 407 merical calculation we use the equality in Eq. (49).

408 Only the electron-phonon interaction and the phonon-  
 409 phonon interaction enter the phase-dependent part of the  
 410 ground-state energy  $\bar{E}_{\phi}$ . It is the quartic order expansion  
 411 term of the electron-phonon interaction and the phonon-  
 412 phonon interaction (also in quartic order of the lattice  
 413 distortion) that relate the phases  $\phi_1, \phi_2$ , and  $\phi_3$  to each  
 414 other and favor a phase difference. Without them chi-  
 415 rality can not be stabilized. Note that the  $2 \times 2 \times 2$ -  
 416 commensurability of the CDW is an important prerequi-  
 417 site for  $\bar{E}_{\phi} \neq 0$ . This rules out incommensurate CDWs  
 418 exhibiting a chiral property.

419 The chiral CDW can be indicated by

$$d_{\phi} = |\delta_{\mathbf{Q}}| |(\phi_1 - \phi_2)(\phi_1 - \phi_3)(\phi_2 - \phi_3)|. \quad (50)$$

420  $d_{\phi}$  is finite only if the CDW is realized and  $\phi_1 \neq \phi_2 \neq \phi_3$ ;  
 421 i.e., it fulfills a prerequisite for an order parameter of the  
 422 chiral CDW.

## D. Phase boundary of the CDW

424 In contrast to the ground-state energy (44) the con-  
 425 straint for the CDW phase boundary can be obtained  
 426 from Eq. (31) without approximations. The derivative of  
 427 the free energy with respect to the static lattice distor-  
 428 tion is needed in the limit  $|\delta_{\mathbf{Q}}| \rightarrow 0$ . To this end, we use  
 429 the ansatz

$$\begin{aligned} E_{\mathbf{k}A} &= \bar{\epsilon}_{\mathbf{k}f} + \sum_{\alpha} |\delta_{\mathbf{Q}}|^2 \bar{A}_{\mathbf{Q}}^f \cos(2\phi_{\alpha}) + |\tilde{\Delta}_{\mathbf{Q}}|^2 d_A \\ &+ \frac{1}{12} \sum_{\alpha} \sum_{\beta \neq \alpha} |\delta_{\mathbf{Q}}|^4 \bar{C}_{\alpha\beta}^f \left[ \cos(2(\phi_{\alpha} - \phi_{\beta}) + \phi_C) \right. \\ &\left. + \cos(2(\phi_{\alpha} + \phi_{\beta}) + \phi_C) \right], \quad (51) \end{aligned}$$

430

$$\begin{aligned}
E_{kB} &= \bar{\epsilon}_{\mathbf{k}+\mathbf{Q}_{11}} + \sum_{\alpha} |\delta_{\mathbf{Q}}|^2 \bar{A}_{\mathbf{Q}}^c \cos(2\phi_{\alpha}) + |\tilde{\Delta}_{\mathbf{Q}}|^2 d_B \\
&+ \frac{1}{12} \sum_{\alpha} \sum_{\beta \neq \alpha} |\delta_{\mathbf{Q}}|^4 \bar{C}_{\alpha\beta}^c \left[ \cos(2(\phi_{\alpha} - \phi_{\beta}) + \phi_C) \right. \\
&\left. + \cos(2(\phi_{\alpha} + \phi_{\beta}) + \phi_C) \right], \quad (52)
\end{aligned}$$

431

$$\begin{aligned}
E_{kC} &= \bar{\epsilon}_{\mathbf{k}+\mathbf{Q}_{22}} + \sum_{\alpha} |\delta_{\mathbf{Q}}|^2 \bar{A}_{\mathbf{Q}}^c \cos(2\phi_{\alpha}) + |\tilde{\Delta}_{\mathbf{Q}}|^2 d_C \\
&+ \frac{1}{12} \sum_{\alpha} \sum_{\beta \neq \alpha} |\delta_{\mathbf{Q}}|^4 \bar{C}_{\alpha\beta}^c \left[ \cos(2(\phi_{\alpha} - \phi_{\beta}) + \phi_C) \right. \\
&\left. + \cos(2(\phi_{\alpha} + \phi_{\beta}) + \phi_C) \right], \quad (53)
\end{aligned}$$

432

$$\begin{aligned}
E_{kD} &= \bar{\epsilon}_{\mathbf{k}+\mathbf{Q}_{33}} + \sum_{\alpha} |\delta_{\mathbf{Q}}|^2 \bar{A}_{\mathbf{Q}}^c \cos(2\phi_{\alpha}) + |\tilde{\Delta}_{\mathbf{Q}}|^2 d_D \\
&+ \frac{1}{12} \sum_{\alpha} \sum_{\beta \neq \alpha} |\delta_{\mathbf{Q}}|^4 \bar{C}_{\alpha\beta}^c \left[ \cos(2(\phi_{\alpha} - \phi_{\beta}) + \phi_C) \right. \\
&\left. + \cos(2(\phi_{\alpha} + \phi_{\beta}) + \phi_C) \right]. \quad (54)
\end{aligned}$$

433 The unknown parameters  $d_{\nu}$ ,  $\nu = A, B, C, D$  can be cal-  
434 culated from the characteristic polynomial of the Hamil-  
435 ton matrix. With the ansatz Eqs. (51)-(54) and Eq. (43),  
436 which also holds up to linear order in the static lattice  
437 distortion, the free energy can be minimized analytically,  
438 which gives the exact result in the limit  $|\delta_{\mathbf{Q}}| \rightarrow 0$ . Con-  
439 sidering this limit the constraint for the CDW phase  
440 boundary is obtained as

$$\begin{aligned}
0 &= \frac{3}{4} \hbar \omega g_{1\mathbf{Q}}^2 + \frac{3}{16} U_{fc} (\hbar \omega)^2 - 3g_{1\mathbf{Q}}^2 [\bar{A}_{\mathbf{Q}}^f n_f + \bar{A}_{\mathbf{Q}}^c (1 - n_f)] \\
&+ \left( g_{1\mathbf{Q}}^2 + \frac{1}{4} U_{fc} \hbar \omega \right)^2 \frac{1}{N} \sum_{\mathbf{k}} \left( \frac{\bar{m}_{E_{\mathbf{k}A}}}{\bar{n}_{E_{\mathbf{k}A}}} \langle n_{\mathbf{k}}^f \rangle \right. \\
&\left. + \frac{\langle n_{\mathbf{k}+\mathbf{Q}_1}^1 \rangle}{\bar{\epsilon}_{\mathbf{k}+\mathbf{Q}_{11}} - \bar{\epsilon}_{\mathbf{k}f}} + \frac{\langle n_{\mathbf{k}+\mathbf{Q}_2}^2 \rangle}{\bar{\epsilon}_{\mathbf{k}+\mathbf{Q}_{22}} - \bar{\epsilon}_{\mathbf{k}f}} + \frac{\langle n_{\mathbf{k}+\mathbf{Q}_3}^3 \rangle}{\bar{\epsilon}_{\mathbf{k}+\mathbf{Q}_{33}} - \bar{\epsilon}_{\mathbf{k}f}} \right), \quad (55)
\end{aligned}$$

441 where

$$\begin{aligned}
\bar{m}_{E_{\mathbf{k}A}} &= \bar{\epsilon}_{\mathbf{k}+\mathbf{Q}_{11}} \bar{\epsilon}_{\mathbf{k}+\mathbf{Q}_{22}} + \bar{\epsilon}_{\mathbf{k}+\mathbf{Q}_{11}} \bar{\epsilon}_{\mathbf{k}+\mathbf{Q}_{33}} + \bar{\epsilon}_{\mathbf{k}+\mathbf{Q}_{22}} \bar{\epsilon}_{\mathbf{k}+\mathbf{Q}_{33}} \\
&+ 3\bar{\epsilon}_{\mathbf{k}f}^2 - 2\bar{\epsilon}_{\mathbf{k}f} (\bar{\epsilon}_{\mathbf{k}+\mathbf{Q}_{11}} + \bar{\epsilon}_{\mathbf{k}+\mathbf{Q}_{22}} + \bar{\epsilon}_{\mathbf{k}+\mathbf{Q}_{33}}), \quad (56) \\
\bar{n}_{E_{\mathbf{k}A}} &= \bar{\epsilon}_{\mathbf{k}f}^3 - \bar{\epsilon}_{\mathbf{k}f}^2 (\bar{\epsilon}_{\mathbf{k}+\mathbf{Q}_{11}} + \bar{\epsilon}_{\mathbf{k}+\mathbf{Q}_{22}} + \bar{\epsilon}_{\mathbf{k}+\mathbf{Q}_{33}}) \\
&+ \bar{\epsilon}_{\mathbf{k}f} (\bar{\epsilon}_{\mathbf{k}+\mathbf{Q}_{11}} \bar{\epsilon}_{\mathbf{k}+\mathbf{Q}_{22}} + \bar{\epsilon}_{\mathbf{k}+\mathbf{Q}_{11}} \bar{\epsilon}_{\mathbf{k}+\mathbf{Q}_{33}} \\
&+ \bar{\epsilon}_{\mathbf{k}+\mathbf{Q}_{22}} \bar{\epsilon}_{\mathbf{k}+\mathbf{Q}_{33}}) - \bar{\epsilon}_{\mathbf{k}+\mathbf{Q}_{11}} \bar{\epsilon}_{\mathbf{k}+\mathbf{Q}_{22}} \bar{\epsilon}_{\mathbf{k}+\mathbf{Q}_{33}}. \quad (57)
\end{aligned}$$

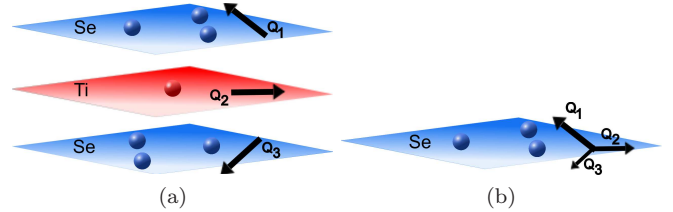
#### 442 E. Characterization of the CDW state in 1T-TiSe<sub>2</sub>

443 Experiments identify a close connection between the  
444 appearance of the CDW state and the periodic lattice

445 displacement in 1T-TiSe<sub>2</sub>.<sup>7</sup> The displacement of the ion  
446  $m$  in the unit cell  $n$  is

$$\tilde{u}(n, m) = \sum_{\alpha} \frac{\hbar}{\sqrt{2M_m\omega}} |\delta_{\mathbf{Q}}| \epsilon(m, \mathbf{Q}_{\alpha}) \cos(\mathbf{Q}_{\alpha} R_n - \phi_{\alpha}), \quad (58)$$

447 where  $\epsilon(m, \mathbf{Q}_{\alpha})$  is the polarization vector and  $M_m$  is the  
448 mass of the ion  $m$ . Clearly each CDW component  $\alpha$   
449 produces a 3D lattice distortion. If  $\phi_1 \neq \phi_2 \neq \phi_3$ , the  
450 lattice will be differently affected by the phonons  $\mathbf{Q}_1$ ,  
451  $\mathbf{Q}_2$ , and  $\mathbf{Q}_3$ . Of course the lattice deformation by the  
452 phonon mode  $\mathbf{Q}_{\alpha}$  is position-dependent; in this way a  
453 complicated distortion pattern of the ions can occur. An  
454 instructive picture can be achieved, however, if one ne-  
455 glects the position-dependence in the  $xy$ -plane. In this  
456 simplified situation, depending on the  $z$ -component as  
457 a function of the position, the magnitude of the lattice  
458 displacement differs along  $\mathbf{Q}_1$ ,  $\mathbf{Q}_2$ , and  $\mathbf{Q}_3$ . As a result  
459 the different ionic layers of 1T-TiSe<sub>2</sub> are dominated by  
460 different phonon modes.<sup>7</sup> The situation where the lower  
461 Se-ion layer is largely affected by the phonon mode  $\mathbf{Q}_3$ ,  
462 the Ti-ion layer by phonons with momentum  $\mathbf{Q}_2$ , and the  
463 upper Se-ion layer by the  $\mathbf{Q}_1$  phonon mode, is illustrated  
464 schematically in Fig. 5(a). Let us consider the upper



465 FIG. 5. (color online) (a) For a chiral ordering the maximum  
466 lattice distortion due to the phonon  $\mathbf{Q}_{\alpha}$  may be located in  
467 different ionic layers. (b) The Se ions in the upper layer are  
468 differently affected by the phonons having momentum  $\mathbf{Q}_1$ ,  
469  $\mathbf{Q}_2$ , or  $\mathbf{Q}_3$ . For further discussion see text.

466 plane of Se ions, which is analyzed in scanning tunneling  
467 microscopy experiments.<sup>5</sup> There, a relative difference of  
468 the phases  $\phi_{\alpha}$  leads, e.g., to a stronger displacement of  
469 the ions in the direction of  $\mathbf{Q}_1$  than in the direction of  
470  $\mathbf{Q}_2$  and  $\mathbf{Q}_3$  [see Fig. 5(b)]. Then the CDW transition  
471 can be viewed as the formation of “virtual layers” with  
472 ordering vectors assigned to a helical structure.<sup>5</sup> This  
473 distortion scenario equates with a fixed phase difference.  
474 Thereby the only crucial parameters are  $\phi_1$ ,  $\phi_2$ , and  $\phi_3$ ;  
475 the finite  $z$  component of the ordering vectors is not a  
476 required prerequisite for the chiral CDW. Although the  
477 different orbital character of the CDW components do  
478 not directly influence the charge modulation, the phase  
479 difference leads to a different transfer of spectral weight  
480 along  $\mathbf{Q}_1$ ,  $\mathbf{Q}_2$ , and  $\mathbf{Q}_3$  and the formation of a chiral CDW  
481 necessarily generates an orbital-ordered state.<sup>8</sup>

482 Equation (40) specifies values for the phases  $\theta_{\alpha}$  and  
483  $\phi_{\alpha}$ . Which particular phase takes one of these values  
484 remains open. For instance, the simultaneous transform-  
485 ations  $\theta_2 \rightarrow \theta_3$  and  $\phi_2 \rightarrow \phi_3$  do not change the energy,  
486



487 but convert a clockwise chiral CDW in an anticlockwise  
488 one. The degeneracy of these two CDW states is in ac-  
489 cord with the experimental findings for  $1T$ -TiSe<sub>2</sub>.<sup>5</sup>

490 As it is apparent in Eq. (43), for finite  $U_{fc}$  and  $g_{1\mathbf{Q}}$   
491 the EI order parameter  $|\Delta_{\mathbf{Q}}| > 0$  if and only if  $|\delta_{\mathbf{Q}}| > 0$ .  
492 This can also be argued on physical grounds. Let us  
493 first consider the case of vanishing electron-phonon cou-  
494 pling. In the EI phase ( $|\Delta_{\mathbf{Q}}| > 0$ ) the system realiz-  
495 es a CDW. When  $g_{1\mathbf{Q}}$  becomes finite in addition, the  
496 lattice adjusts commensurate with the electron density  
497 modulation. Hence, in this case, any finite  $g_{1\mathbf{Q}}$  im-  
498 mediately results in  $|\delta_{\mathbf{Q}}| > 0$ . On the other hand,  
499 at vanishing Coulomb interaction but sufficiently large  
500  $g_{1\mathbf{Q}} > g_{1\mathbf{Q},c}$ , a lattice instability develops leading to a  
501 finite  $\sum_{\mathbf{k}} \langle c_{\mathbf{k}+\mathbf{Q}\alpha}^\dagger f_{\mathbf{k}} \rangle$ . This hybridization parameter enters  
502 the explicit equation for the EI order parameter, see  
503 Eq. (12).  $|\Delta_{\mathbf{Q}}| > 0$  then follows from any finite Coulomb  
504 interaction. Our approach therefore does not discrim-  
505 inate between an excitonic and phonon-driven instabil-  
506 ity if both electron-electron and electron-phonon interac-  
507 tions are at play.

### 508 III. NUMERICAL RESULTS

#### 509 A. Model assumptions

510 In view of the quasi-2D crystallographic and electronic  
511 structure of  $1T$ -TiSe<sub>2</sub>, and in order to simplify the nu-  
512 merics, we restrict the following analysis to a strictly 2D  
513 setting. Moreover, being close to the Fermi energy, we  
514 will approximate the bands parabolically:<sup>10</sup>

$$\varepsilon_{\mathbf{k}f} = -t_f(k_x^2 + k_y^2), \quad (59)$$

$$\varepsilon_{\mathbf{k}1} = t_c^x(k_x - Q_{1x})^2 + t_c^y(k_y - Q_{1y})^2 + E_c, \quad (60)$$

515 with hopping amplitudes  $t_f$ ,  $t_c^x$ , and  $t_c^y$ . The other two  
516 conduction bands  $\varepsilon_{\mathbf{k}2}$  and  $\varepsilon_{\mathbf{k}3}$  have analogous dispersions,  
517 but the momenta are rotated by  $2\pi/3$  and  $4\pi/3$ , respec-  
518 tively. All three conduction bands share the same mini-  
519 mum  $E_c$ , see Fig. 3.

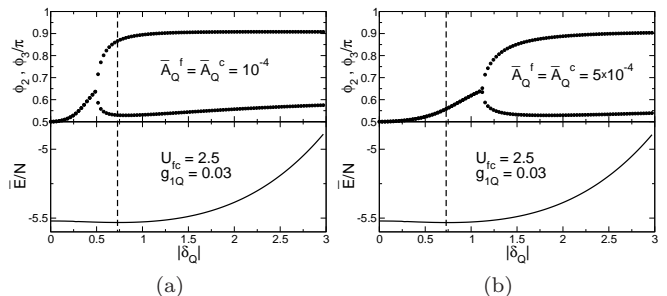
520 From the band dispersion provided by Monney *et al.*  
521 in Ref. 10 we derive  $t_f = 1.3$  eV, which will be taken as  
522 the unit of energy hereafter, and  $t_c^x = 0.042$  and  $t_c^y =$   
523  $0.105$ . The bare phonon frequency is estimated as  $\hbar\omega =$   
524  $0.013$ , in accordance with the value given by Weber *et*  
525 *al.* in Ref. 20. Furthermore, we set  $E_c = -3.30$  and  
526  $U_{cc} = U_{fc} + 1.0$ . Note that  $E_c$  is the minimum of the  
527 bare conduction band. The effective band overlap will  
528 be significantly smaller due to the Coulomb interaction  
529 induced Hartree shift. If it is not explicitly noted we take  
530  $\hat{B}_{1\mathbf{Q}}^\alpha = 0.5 \times 10^{-4}$ ,  $\hat{B}_{2\mathbf{Q}} = 10^{-4}$ ,  $\bar{C}_{\alpha\beta}^f = \bar{C}_{\alpha\beta}^c = 8.5 \times 10^{-4}$ ,  
531  $\hat{D} = 10^{-5}$ , and  $\phi_C = 3\pi/10$ .

532 The self-consistency loop, comprising the determina-  
533 tion of the total and partial particle densities and the  
534 chemical potential, is solved iteratively until the relative  
535 error of each physical quantity is less than  $10^{-6}$ . The nu-

536 merical integrations were performed using the Cubpack  
537 package.<sup>49</sup>

#### 538 B. Formation scenario of the chiral CDW

539 We start with the analysis of the ground-state energy  
540 ( $T = 0$ ), where we treat the static lattice distortion as a  
541 variational parameter. Without loss of generality we  
542 choose  $\phi_1 = \pi/2$ . The other phases  $\phi_2$  and  $\phi_3$  are de-  
543 termined by minimizing  $\bar{E}_\phi/N$  using a simplex method.  
544 The results for  $U_{fc} = 2.5$  and  $g_{1\mathbf{Q}} = 0.03$  are shown in  
545 Fig. 6.



546 FIG. 6. (Upper panels) Phases and (lower panels) ground-  
547 state energy as a function of the static lattice distortion. The  
548 dashed lines designate the physical value of the static lattice  
549 distortion. We set  $\phi_1 = \pi/2$  and the interband Coulomb  
550 interaction is  $U_{fc} = 2.5$ . For the electron-phonon interaction  
551 we take  $g_{1\mathbf{Q}} = 0.03$ , (a)  $\bar{A}_{\mathbf{Q}}^f = \bar{A}_{\mathbf{Q}}^c = 10^{-4}$ , and (b)  $\bar{A}_{\mathbf{Q}}^f =$   
552  $\bar{A}_{\mathbf{Q}}^c = 5 \times 10^{-4}$ .

548 Since we assumed the nonlinear electron-phonon and  
549 the phonon-phonon interaction constants are much  
550 smaller than  $U_{fc}$ ,  $U_{cc}$ , and  $g_{1\mathbf{Q}}$ , the energy  $\bar{E}/N \approx \bar{E}_\delta/N$   
551 and the (physical) static lattice distortion, given by the  
552 dashed lines in Figs. 6, is primarily determined by the  
553 Coulomb interaction and  $g_{1\mathbf{Q}}$ .

554 We find a complex formation scenario for the chi-  
555 ral property. For  $|\delta_{\mathbf{Q}}| \rightarrow 0$  all phases are equal, i.e.,  
556  $\phi_1 = \phi_2 = \phi_3 = \pi/2$  and the CDW is nonchiral. With  
557 growing static lattice distortion  $\phi_2 = \phi_3 \neq \phi_1$ . Com-  
558 pared with the normal phase and the limit  $|\delta_{\mathbf{Q}}| \rightarrow 0$  the  
559 mirror symmetry is reduced in this state. However, there  
560 exists a mirror symmetry along  $\mathbf{Q}_1$  (cf. Fig. 1), and the  
561 CDW is still nonchiral. If the static lattice distortion  
562 exceeds a threshold, chirality sets in and  $\phi_1 \neq \phi_2 \neq \phi_3$ .

563 With increasing  $\bar{A}_{\mathbf{Q}}^{f(c)}$  the threshold for the static lat-  
564 tice distortion that separates the chiral and the nonchiral  
565 CDW grows, see Fig. 7. The electron-phonon interaction  
566 constant  $g_{1\mathbf{Q}}$  barely influences the chiral property of the  
567 CDW.

569 The scenario shown in Fig. 6 suggests that coming  
570 from the uniform, high temperature phase and lower-  
571 ing  $T$  there is first a transition to the nonchiral CDW  
572 at  $T_{\text{nonchiral CDW}}$ . Chirality is formed at  $T_{\text{chiral CDW}} <$   
573  $T_{\text{nonchiral CDW}}$ . This sequence of transitions agrees with

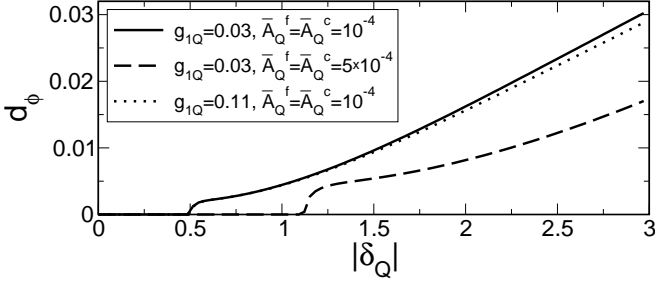


FIG. 7. Chiral-CDW characteristic quantity  $d_\phi$  as a function of the static lattice distortion. The solid line represents the result for  $g_{1\mathbf{Q}} = 0.03$  and  $\bar{A}_{\mathbf{Q}}^f = \bar{A}_{\mathbf{Q}}^c = 10^{-4}$ , the long-dashed line is the result for  $g_{1\mathbf{Q}} = 0.03$  and  $\bar{A}_{\mathbf{Q}}^f = \bar{A}_{\mathbf{Q}}^c = 5 \times 10^{-4}$ , and the dotted line shows the result for  $g_{1\mathbf{Q}} = 0.11$  and  $\bar{A}_{\mathbf{Q}}^f = \bar{A}_{\mathbf{Q}}^c = 10^{-4}$ .

574 the result from the Landau-Ginzburg approach<sup>7,8</sup> and  
 575 is supported by very recent x-ray diffraction and elec-  
 576 trical transport measurements.<sup>50</sup> The difference between  
 577  $T_{\text{nonchiralCDW}}$  and  $T_{\text{chiralCDW}}$  is estimated experimen-  
 578 tally to be less than 10 K. Moreover, the suggested transi-  
 579 tion scenario does not contradict experiment, where  $1T$ -  
 580  $\text{TiSe}_2$  is gradually doped with Cu until the CDW is sup-  
 581 pressed in favor of a superconducting phase.<sup>51</sup> Here, chi-  
 582 rality is present until the breakdown of the CDW. Since  
 583 the transition from the CDW to the superconducting  
 584 phase is affirmed as a first order transition,<sup>52</sup>  $|\delta_{\mathbf{Q}}|$  does  
 585 not have to be small at the phase boundary and chirality  
 586 may exist.

To combine our approach with the Landau-Ginzburg  
 treatment we set  $\hat{B}_{1\mathbf{Q}}^\alpha = 0$ ,  $\hat{D} = 0$ , neglect the terms  
 $\cos(2(\phi_\alpha + \phi_\beta) + \phi_C)$ , and set  $\phi_C = 0$ . Our model then  
 reproduces the functional dependency of the free energy  
 functional in Refs. 7 and 8. The Landau-Ginzburg param-  
 eters can then be expressed as

$$\frac{3}{2}a_0 = -\frac{3}{4}\hbar\omega - \frac{3}{16}U_{fc}\left(\frac{\hbar\omega}{g_{1\mathbf{Q}}}\right)^2, \quad (61)$$

$$\frac{1}{2}a_1(1 - \gamma) = \bar{A}_{\mathbf{Q}}^f n_f + \bar{A}_{\mathbf{Q}}^c (1 - n_f), \quad (62)$$

$$\frac{3}{8}(15c_0 + 8d_0) = 3\tilde{D} - \hat{B}_{2\mathbf{Q}}\frac{\hbar\omega}{g_{1\mathbf{Q}}}, \quad (63)$$

$$\frac{3}{4}c_2 = \bar{C}_{\alpha\beta}^f n_f + \bar{C}_{\alpha\beta}^c (1 - n_f). \quad (64)$$

588 Figure 8(a) shows an example for this scheme. Note  
 589 that the phases  $\phi_\alpha$  are periodic with  $\pi$  and Fig. 8(a)  
 590 shows that  $\phi_2 = -\phi_3$ , which was obtained analytically in  
 591 Refs. 7 and 8. Most notably, if the  $\cos(2(\phi_\alpha + \phi_\beta) + \phi_C)$   
 592 contribution and the phase  $\phi_C$  are neglected the “inter-  
 593 mediate” state where  $\phi_2 = \phi_3 \neq \phi_1$  is missing. The  
 594 chiral CDW emerges directly from the nonchiral CDW,  
 595 where  $\phi_1 = \phi_2 = \phi_3 = \pi/2$ . The comparison of the  
 596 phase-dependent part  $\bar{E}_\phi/N$  shows that the approxima-  
 597 tion provided by Eq. (46) exhibits the lower energy. The

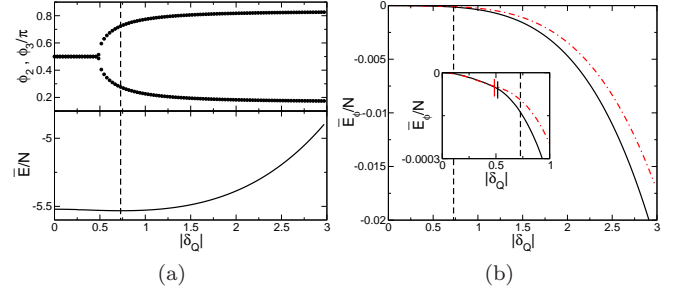


FIG. 8. (color online) (a) Phases and ground-state energy as a function of the static lattice distortion, where the functional dependency on the phases  $\phi_\alpha$  is assumed as in Refs. 7 and 8. (b) Comparison of the phase-dependent part of the ground-state energy Eq. (46) (black solid line) and the counterpart for the phase dependency as suggested by van Wezel<sup>7,8</sup> (red dot-dashed line). The small vertical lines in the inset indicate the critical  $|\delta_{\mathbf{Q}}|$  for the onset of chirality in the respective approximation scheme. In both figures the dashed line designates the physical value of the static lattice distortion. The model parameters are  $U_{fc} = 2.5$ ,  $g_{1\mathbf{Q}} = 0.03$ ,  $\bar{A}_{\mathbf{Q}}^f = \bar{A}_{\mathbf{Q}}^c = 10^{-4}$ .

598 onset of the chiral CDW differs only slightly between the  
 599 two approximation schemes.

### C. Phase diagram of the mEFKM

601 To set the stage for the analysis of the interplay of  
 602 Coulomb and electron-phonon interaction effects we first  
 603 discuss the phase diagram of the pure mEFKM, cf. Fig. 9.  
 604 Here, since  $g_{1\mathbf{Q}} = 0$  (and as a result  $\delta_{\mathbf{Q}\alpha} = 0$ ), the EI  
 605 low-temperature phase typifies a normal CDW. As for  
 606 the EFKM on a square lattice (see inset), at  $T = 0$  we  
 607 find a finite critical Coulomb strength above which the  
 608 EI phase does not exist. This is because the large band  
 609 splitting caused by the Hartree term of the Coulomb in-  
 610 teraction prevents  $c$ - $f$  electron coherence.<sup>42</sup> In contrast

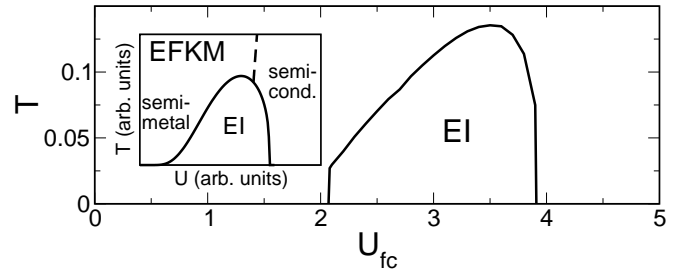


FIG. 9. Phase diagram of the mEFKM. The inset displays the schematic phase diagram of the simplified two-band EFKM on a square lattice according to Ref. 42.

612 to the EFKM, in our four-band model we also find a  
 613 critical lower Coulomb strength for the EI phase. This  
 614 can be understood as follows: since the valence band  
 615 is isotropic while the conduction-band dispersions are  
 616 strongly anisotropic, particles close to the Fermi level  
 617

do not find a large number of partners with appropriate momentum for electron-hole pairing. Thus, for  $U_{fc}$  smaller than a critical Coulomb attraction, the amount of energy to create a macroscopic number of excitons is larger than the energy gain from the condensation transition into the EI state. Therefore the system remains in the semimetallic phase.<sup>53</sup> The rather abrupt increase of the critical temperature at the lower critical Coulomb interaction is due to the degeneracy of the conduction bands and the particular anisotropy used.

#### D. Influence of the lattice degrees of freedom

We now analyze the situation when phonons participate in the CDW formation. In Fig. 10 the critical temperatures for  $g_{1\mathbf{Q}} = 0.03$  and  $g_{1\mathbf{Q}} = 0.11$  can be found. For very small electron-phonon coupling the phase dia-

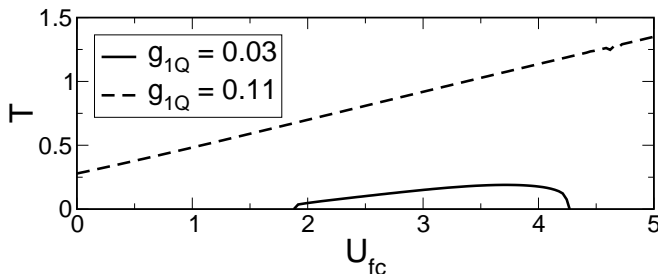


FIG. 10. CDW phase boundaries for  $g_{1\mathbf{Q}} = 0.03$  (solid line) and  $g_{1\mathbf{Q}} = 0.11$  (dashed line).

gram resembles the situation for the mEFKM. As the interaction strength  $g_{1\mathbf{Q}}$  increases the situation changes dramatically. For sufficiently large electron-phonon couplings, we no longer find critical lower and upper values  $U_{fc}$  for the CDW transition and the transition temperature increases linearly with  $U_{fc}$ . That is the critical temperature is significantly enhanced by  $g_{1\mathbf{Q}}$ . Evidently electron-hole attraction and electron-phonon coupling act together in the formation of a very stable CDW phase.

The impact of the Coulomb interaction and the electron-phonon interaction is summarized by the ground-state phase diagram shown in Fig. 11. For weak electron-phonon couplings  $g_{1\mathbf{Q}}$  the CDW is mainly driven by the Coulomb attraction  $U_{fc}$  between electrons and holes. The greater  $g_{1\mathbf{Q}}$ , the larger the region where the CDW is stable. For  $g_{1\mathbf{Q}} > 0.09$  the electron-phonon coupling alone can cause the CDW transition, even at  $U_{fc} = 0$  (blue line in Fig. 11). Depending primarily on the magnitude of the static lattice distortion the CDW can be chiral in this limit, whereas the CDW in the opposite EI limit does not exhibit chirality ( $g_{1\mathbf{Q}} = 0$ , red line in Fig. 11).

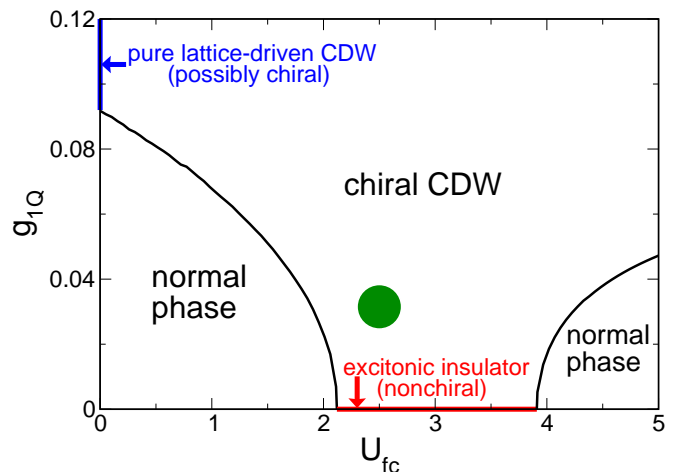


FIG. 11. (color online) Ground-state phase diagram of the mEFKM with additional electron-phonon coupling. The CDW phase is characterized by a finite gap parameter  $|\hat{\Delta}_{\mathbf{Q}}|$ . The red line at  $g_{1\mathbf{Q}} = 0$  marks the EI phase of the pure mEFKM. The blue line at  $U_{fc} = 0$  refers to a CDW induced solely by the electron-lattice interaction. The green point designates the range of model parameters appropriate for  $1T$ -TiSe<sub>2</sub>.

#### E. Relation to $1T$ -TiSe<sub>2</sub>

Based on the phase diagram derived for the mEFKM with electron-phonon coupling, we now attempt to estimate the electron-electron and electron-phonon interaction constants,  $U_{fc}$  and  $g_{1\mathbf{Q}}$ , for  $1T$ -TiSe<sub>2</sub>. To make contact with experiments we take the displacements of the Ti ions measured by Di Salvo *et al.*:  $\tilde{u}(n, m = \text{Ti}) = 0.04\text{\AA}$ .<sup>4</sup> Then, from Eq. (58), we can specify the value of  $|\delta_{\mathbf{Q}}|$ . For  $1T$ -TiSe<sub>2</sub>, the gap parameter was determined experimentally as 120 meV by Monney *et al.*; see Ref. 44. Adjusting this value to our theoretical results yields  $U_{fc} \approx 2.5$  ( $\approx 3$  eV) and  $g_{1\mathbf{Q}} \approx 0.03$  ( $\approx 0.04$  eV); see the green marker in Fig. 11. For these values both the theoretical ion displacement and gap parameter are in the same order of magnitude as the measured ones. Using  $U_{fc} \approx 2.5$  for  $1T$ -TiSe<sub>2</sub>, the electron-hole pairing is BCS-like. Since  $g_{1\mathbf{Q}} \simeq 0.03$  is too small to cause a CDW for vanishing Coulomb interaction and, as discussed above, the EI scenario alone will not yield a stable chiral CDW, our results are in favor of a combined lattice-deformation/EI mechanism for the experimentally observed chiral CDW transition, as suggested in Refs. 22 and 54.

## IV. CONCLUSIONS

In this work we have argued how the observed chiral charge-density-wave (CDW) phase in  $1T$ -TiSe<sub>2</sub> may be stabilized. In the framework of the multiband extended Falicov-Kimball model (mEFKM) we showed that a purely electronic—exciton pairing and condensation—

mechanism is insufficient to induce the observed (long-ranged) chiral charge order. We propose that the coupling of the electrons to the lattice degrees of freedom is essential for the formation of a chiral CDW state.

We note that in our model clockwise and anticlockwise CDWs are degenerate. This is in accord with experimental findings.<sup>5</sup> The chiral property can properly be observed in the ionic displacements accompanying the CDW in  $1T$ -TiSe<sub>2</sub>.

Whether the chiral CDW is stabilized depends particularly on the magnitude of the static lattice distortion and also on the ratios of the electron-phonon, respectively the phonon-phonon, interaction constants. Our analysis confirms the sequential transition scenario  $T_{\text{chiral CDW}} < T_{\text{nonchiral CDW}}$  as was proposed in Refs. 7 and 8 and corroborated experimentally.<sup>50</sup> However, we extended this scenario by the inclusion of further interactions. This leads to a CDW state for  $T_{\text{chiral CDW}} < T < T_{\text{nonchiral CDW}}$ , where the mirror symmetry is reduced compared to the normal phase, but chirality is not yet formed.

Concerning the microscopic mechanism underlying the CDW transition, we demonstrated that electron-electron interaction and electron-phonon coupling support each other in driving the electron-hole pairing and finally the instability. This suggests that the CDW transition in  $1T$ -TiSe<sub>2</sub> is due to a combined lattice distortion and exciton-condensation effect. The outcome is a spontaneous broken-symmetry CDW low-temperature state with small but finite lattice deformation. Of course, both the mean-field treatment of the Coulomb interaction and the frozen-phonon approach are rather crude approxima-

tions and a more elaborated study of the complex interplay between the electronic and phononic degrees of freedom is highly desirable to confirm our proposed scenario for the chiral CDW transition in  $1T$ -TiSe<sub>2</sub>.

Let us finally point out that we called  $|\Delta_{\mathbf{Q}}|$  the excitonic-insulator order parameter on account of its analog in the EFKM.<sup>35–42</sup> The meaning of a finite  $|\Delta_{\mathbf{Q}}|$  in the presence of a band coupling is imprecise however. Likewise a spontaneous hybridization of the valence band with one of the conduction bands, signaling the exciton condensate in the mEFKM, may be induced by a sufficiently large electron-phonon coupling  $g_{1\mathbf{Q}}$ . A general criterion for the formation of an exciton condensate in a strongly coupled band situation has not been established to date. This is an open issue which deserves further analysis because of its relevance in characterizing the nature of CDW transitions also in other materials.<sup>55,56</sup>

## ACKNOWLEDGMENTS

We thank P. Aebi, K. W. Becker, F. X. Bronold, D. Ihle, G. Monney, and N. V. Phan for valuable discussions. This work is supported by the Deutsche Forschungsgemeinschaft through SFB 652 (project B5), by the Fonds National Suisse pour la Recherche Scientifique through Div. II, the Swiss National Center of Competence in Research MaNEP, and the U.S. Department of Energy. C.M. acknowledges also support by the Fonds National Suisse pour la Recherche Scientifique under grant PA00P2-142054.

<sup>1</sup> R. Peierls, *Quantum theory of solids* (Oxford University Press, Oxford, 1955).

<sup>2</sup> J. Sólyom, *Adv. Phys.* **28**, 201 (1979).

<sup>3</sup> G. Grüner, *Density Waves in Solids* (Perseus Publishing, 2000).

<sup>4</sup> F. J. Di Salvo, D. E. Moncton, and J. V. Waszczak, *Phys. Rev. B* **14**, 4321 (1976).

<sup>5</sup> J. Ishioka, Y. H. Liu, K. Shimatake, T. Kurosawa, K. Ichimura, Y. Toda, M. Oda, and S. Tanda, *Phys. Rev. Lett.* **105**, 176401 (2010).

<sup>6</sup> J. van Wezel and P. Littlewood, *Physics* **3**, 87 (2010).

<sup>7</sup> J. van Wezel, *Europhys. Lett.* **96**, 67011 (2011).

<sup>8</sup> J. van Wezel, *Physica B* **407**, 1779 (2012).

<sup>9</sup> H. Cercellier, C. Monney, F. Clerc, C. Battaglia, L. Despont, M. G. Garnier, H. Beck, P. A. ans L. Patthey, H. Berger, and L. Forró, *Phys. Rev. Lett.* **99**, 146403 (2007).

<sup>10</sup> C. Monney, H. Cercellier, F. Clerc, C. Battaglia, E. F. Schwier, C. Didiot, M. G. Garnier, H. Beck, P. Aebi, H. Berger, L. Forró, and L. Patthey, *Phys. Rev. B* **79**, 045116 (2009).

<sup>11</sup> C. Monney, C. Battaglia, H. Cercellier, P. Aebi, and H. Beck, *Phys. Rev. Lett.* **106**, 106404 (2011).

<sup>12</sup> M. M. May, C. Brabetz, C. Janowitz, and R. Manzke,

*Phys. Rev. Lett.* **107**, 176405 (2011).

<sup>13</sup> T. Rohwer, S. Hellmann, M. Wiesenmayer, C. Sohrt, A. Stange, B. Slomski, A. Carr, Y. Liu, L. M. Avila, M. Kalläne, S. Mathias, L. Kipp, K. Rossnagel, and M. Bauer, *Nature* **471**, 490 (2011).

<sup>14</sup> H. P. Hughes, *J. Phys. C* **10**, L319 (1977).

<sup>15</sup> K. Rossnagel, L. Kipp, and M. Skibowski, *Phys. Rev. B* **65**, 235101 (2002).

<sup>16</sup> Y. Yoshida and K. Motizuki, *J. Phys. Soc. Japan* **49**, 898 (1980).

<sup>17</sup> K. Motizuki, N. Suzuki, Y. Yoshida, and Y. Takaoka, *Solid State Commun.* **40**, 995 (1981).

<sup>18</sup> N. Suzuki, A. Yamamoto, and K. Motizuki, *J. Phys. Soc. Japan* **54**, 4668 (1985).

<sup>19</sup> M. Holt, P. Zschack, H. Hong, M. Y. Chou, and T. C. Chiang, *Phys. Rev. Lett.* **86**, 3799 (2001).

<sup>20</sup> F. Weber, S. Rosenkranz, J.-P. Castellán, R. Osborn, G. Karapetrov, R. Hott, R. Heid, K.-P. Bohnen, and A. Alatas, *Phys. Rev. Lett.* **107**, 266401 (2011).

<sup>21</sup> M. Calandra and F. Mauri, *Phys. Rev. Lett.* **106**, 196406 (2011).

<sup>22</sup> J. van Wezel, P. Nahai-Williamson, and S. S. Saxena, *Europhys. Lett.* **89**, 47004 (2010).

<sup>23</sup> C. Monney, G. Monney, P. Aebi, and H. Beck, *New J.*

- 795 Phys. **14**, 075026 (2012).  
796 <sup>24</sup> J. Neuenschwander and P. Wachter, Phys. Rev. B **41**,  
797 12693 (1990).  
798 <sup>25</sup> P. Wachter and B. Bucher, Physica B **408**, 51 (2013).  
799 <sup>26</sup> K. Kanda, K. Machida, and T. Matsubara, Solid State  
800 Commun. **19**, 651 (1976).  
801 <sup>27</sup> T. Portengen, T. Östreich, and L. J. Sham, Phys. Rev.  
802 Lett. **76**, 3384 (1996).  
803 <sup>28</sup> C. D. Batista, Phys. Rev. Lett. **89**, 166403 (2002).  
804 <sup>29</sup> N. F. Mott, Philos. Mag. **6**, 287 (1961).  
805 <sup>30</sup> R. Knox, in *Solid State Physics*, edited by F. Seitz and  
806 D. Turnbull (Academic Press, New York, 1963) p. Suppl.  
807 5 p. 100.  
808 <sup>31</sup> D. Jérôme, T. M. Rice, and W. Kohn, Physical Review  
809 **158**, 462 (1967).  
810 <sup>32</sup> F. X. Bronold and H. Fehske, Phys. Rev. B **74**, 165107  
811 (2006).  
812 <sup>33</sup> C. D. Batista, J. E. Gubernatis, J. Bonča, and H. Q. Lin,  
813 Phys. Rev. Lett. **92**, 187601 (2004).  
814 <sup>34</sup> P. Farkašovský, Phys. Rev. B **77**, 155130 (2008).  
815 <sup>35</sup> C. Schneider and G. Czycholl, Eur. Phys. J. B **64**, 43  
816 (2008).  
817 <sup>36</sup> D. Ihle, M. Pfafferott, E. Burovski, F. X. Bronold, and  
818 H. Fehske, Phys. Rev. B **78**, 193103 (2008).  
819 <sup>37</sup> B. Zenker, D. Ihle, F. X. Bronold, and H. Fehske, Phys.  
820 Rev. B **81**, 115122 (2010).  
821 <sup>38</sup> N. V. Phan, K. W. Becker, and H. Fehske, Phys. Rev. B  
822 **81**, 205117 (2010).  
823 <sup>39</sup> B. Zenker, D. Ihle, F. X. Bronold, and H. Fehske, Phys.  
824 Rev. B **83**, 235123 (2011).  
825 <sup>40</sup> N. V. Phan, H. Fehske, and K. W. Becker, Europhys. Lett.  
826 **95**, 17006 (2011).  
827 <sup>41</sup> K. Seki, R. Eder, and Y. Ohta, Phys. Rev. B **84**, 245106  
828 (2011).  
829 <sup>42</sup> B. Zenker, D. Ihle, F. X. Bronold, and H. Fehske, Phys.  
830 Rev. B **85**, 121102R (2012).  
831 <sup>43</sup> C. Monney, E. F. Schwier, M. G. Garnier, N. Mariotti,  
832 C. Didiot, H. Cercellier, J. Marcus, H. Berger, A. N. Titov,  
833 H. Beck, and P. Aebi, New J. Phys. **12**, 125019 (2010).  
834 <sup>44</sup> C. Monney, E. F. Schwier, M. G. Garnier, N. Mariotti,  
835 C. Didiot, H. Beck, P. Aebi, C. Cercellier, J. Marcus,  
836 C. Battaglia, H. Berger, and A. N. Titov, Phys. Rev. B  
837 **81**, 155104 (2010).  
838 <sup>45</sup> M. Cazzaniga, H. Cercellier, M. Holzmann, C. Monney,  
839 P. Aebi, G. Onida, and V. Olevano, Phys. Rev. B **85**,  
840 195111 (2012).  
841 <sup>46</sup> C. Monney, G. Monney, P. Aebi, and H. Beck, Phys. Rev.  
842 B **85**, 235150 (2012).  
843 <sup>47</sup> J. M. Ziman, *Electrons and Phonons* (Clarendon, London,  
844 1960).  
845 <sup>48</sup> N. W. Ashcroft and N. D. Mermin, *Solid state physics*  
846 (Saunders College Publ. Philadelphia, 1976).  
847 <sup>49</sup> R. Cools and A. Haegemans, ACM Transactions on Math-  
848 ematical Software **29**, 287 (2003).  
849 <sup>50</sup> J.-P. Castellan, S. Rosenkranz, R. Osborn, Q. Li, K. Gray,  
850 G. Karapetrov, J. Ruff, and J. van Wezel, (2012),  
851 preprint.  
852 <sup>51</sup> M. Iavarone, R. di Capua, X. Zhang, M. Golalikhani, S. A.  
853 Moore, and G. Karapetrov, Phys. Rev. B **85**, 155103  
854 (2012).  
855 <sup>52</sup> E. Morosan, H. W. Zandbergen, B. S. Dennis, J. W. G.  
856 Bos, Y. Onose, T. Klimczuk, A. P. Ramirez, N. P. Ong,  
857 and R. J. Cava, Nature Phys. **2**, 544 (2006).  
858 <sup>53</sup> J. Zittartz, Phys. Rev. **162**, 752 (1967).  
859 <sup>54</sup> Z. Zhu, Y. Cheng, and U. Schwingenschlögl, Phys. Rev.  
860 B **85**, 245133 (2012).  
861 <sup>55</sup> T. Kaneko, T. Toriyama, T. Konishi, and Y. Ohta, Phys.  
862 Rev. B **87**, 035121 (2013), *ibid*, **87**, 199902(E) (2013).  
863 <sup>56</sup> D. K. Efimkin, Y. E. Lozovik, and A. A. Sokolik, Phys.  
864 Rev. B **86**, 115436 (2012).